A MODEL FOR PREDICTING THE SPECTRAL IRRADIANCE ON A GROUND TARGET FROM THE SUN AND THE CLEAR DAYTIME SKY

Alan R. Downs

Ballistic Research Laboratories
Aberdeen Proving Ground, Maryland

September 1972

BRL MR 2221

BRL

AD

MEMORANDUM REPORT NO. 2221

A MODEL FOR PREDICTING THE SPECTRAL IRRADIANCE ON A GROUND TARGET FROM THE SUN AND THE CLEAR DAYTIME SKY

by

Alan R. Downs

September 1972

BALLISTIC RESEARCH LABORATORIES
ABERDEEN PROVING GROUND, MARYLAND

Destroy this report when it is no longer needed.
Do not return it to the originator.

Secondary distribution of this report by originating or sponsoring activity is prohibited.

Additional copies of this report may be purchased from the U.S. Department of Commerce, National Technical Information Service, Springfield, Virginia 22151

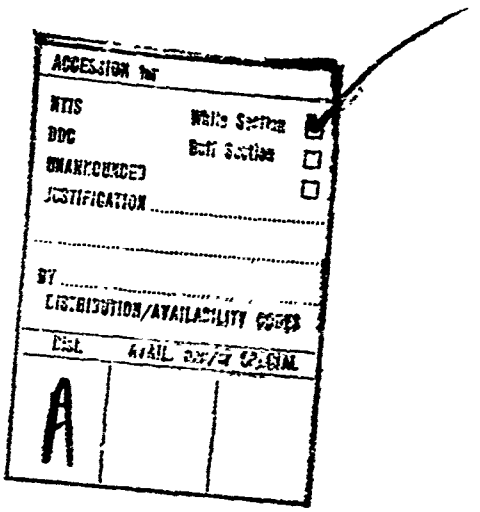

The findings in this report are not to be construed as an official Department of the Army position, unless so designated by other authorized documents.

Unclassified
Security Classification

DOCUMENT CONTROL DATA - R & D

(Security classification of title, body of abstract and indexing annotation must be entered when the overall report is classified)

1. ORIGINATING ACTIVITY (Corporate author)
U. S. Army Ballistic Research Laboratories
Aberdeen Proving Ground, Maryland

2a. REPORT SECURITY CLASSIFICATION
Unclassified
2b. GROUP

3. REPORT TITLE
A MODEL FOR PREDICTING THE SPECTRAL IRRADIANCE ON A GROUND TARGET FROM THE SUN AND THE CLEAR DAYTIME SKY

4. DESCRIPTIVE NOTES (Type of report and inclusive dates)

5. AUTHOR(S) (First name, middle initial, last name)
Alan R. Downs

6. REPORT DATE	7a. TOTAL NO. OF PAGES	7b. NO. OF REFS
September 1972	67 61	18

8a. CONTRACT OR GRANT NO.	9a. ORIGINATOR'S REPORT NUMBER(S)
b. PROJECT NO. RDT&E 1T061102B11A	BRL Memorandum Report No. 2221
c.	9b. OTHER REPORT NO(S) (Any other numbers that may be assigned this report)
d.	

10. DISTRIBUTION STATEMENT
Approved for public release; distribution unlimited.

11. SUPPLEMENTARY NOTES	12. SPONSORING MILITARY ACTIVITY
	U.S. Army Materiel Command Washington, D.C. 20315

13. ABSTRACT

A single-scattering atmospheric radiative transfer model is derived and described. This model, based only on ground level measurements, can be used to predict the spectral and directional characteristics of radiation incident on a ground target from the sun and the cloudless daytime in the absence of discontinuities such as inversion layers. Wavelengths from 0.4 to 1.7 microns are considered.

The model makes use of available information on the scattering and absorbing properties of atmospheric constituents and the distribution of these constituents with altitude. The final result is in the form of a function that can be integrated by computer to determine the spectral irradiance on the target from a preselected segment of the clear daytime sky. Detailed discussions of error sources and model limitations are included.

DD FORM 1 NOV 68 1473 REPLACES DD FORM 1472, 1 JAN 64, WHICH IS OBSOLETE FOR ARMY USE.

Unclassified
Security Classification

14. KEY WORDS	LINK A		LINK B		LINK C	
	ROLE	WT	ROLE	WT	ROLE	WT
Scattering						
Absorption						
Target Signature						
Predictive Modeling						

BALLISTIC RESEARCH LABORATORIES

MEMORANDUM REPORT NO. 2221

SEPTEMBER 1972

A MODEL FOR PREDICTING THE SPECTRAL IRRADIANCE ON A GROUND TARGET FROM THE SUN AND THE CLEAR DAYTIME SKY

Alan R. Downs

Concepts Analysis Laboratory

RDT&E Project No. 1T061102B11A

ABERDEEN PROVING GROUND, MARYLAND

BALLISTIC RESEARCH LABORATORIES

MEMORANDUM REPORT NO. 2221

ARDowns/jdk
Aberdeen Proving Ground, Md.
September 1972

A MODEL FOR PREDICTING THE SPECTRAL IRRADIANCE ON A GROUND TARGET FROM THE SUN AND THE CLEAR DAYTIME SKY

ABSTRACT

A single-scattering atmospheric radiative transfer model is derived and described. This model, based only on ground level measurements, can be used to predict the spectral and directional characteristics of radiation incident on a ground target from the sun and the cloudless daytime sky in the absence of discontinuities such as inversion layers. Wavelengths from 0.4 to 1.7 microns are considered.

The model makes use of available information on the scattering and absorbing properties of atmospheric constituents and the distribution of these constituents with altitude. The final result is in the form of a function that can be integrated by computer to determine the spectral irradiance on the target from a preselected segment of the clear daytime sky. Detailed discussions of error sources and model limitations are included.

TABLE OF CONTENTS

LIST OF ILLUSTRATIONS

LIST OF ILLUSTRATIONS (CONT.)

I. BACKGROUND

Reflectance modeling for natural sources of irradiation is a part of a comprehensive ground target signature modeling program. The objective of this research is to develop a unified methodology, vis. predictive and empirical modeling of the basic fundamental physical phenomena that are involved in the application of ground target and background signatures to the design and evaluation of target acquisition systems, terminal homing systems and countermeasures.

The natural sources of irradiation to be considered include the sun, sky and ground during the day and the moon, sky and ground at night. The precedure to be followed in modeling these sources is the same for the daytime and nighttime cases except that at night an airglow term must be added to the sky input. The wavelengths of interest start in the visual part of the spectrum (0.4 micron) and extend to the wavelength at which reflected energy is negligible compared to the emitted energy. This upper wavelength has been selected to be 3.5 microns. The wavelength increment must be small enough to permit sensor optimization studies to be performed but large enough that the data handling procedure does not become too complicated. The wavelength increment selected for this program is 0.05 micron. For simplicity, only single scattering has been considered. The effect of multiple scattering can be large in some cases and will therefore be addressed later in the program.

Once the sources are adequately characterized, the radiation-target interaction must be considered. The only phenomenon treated in this portion of the program is reflection. It is necessary to know the bidirectional reflection characteristics of target components as a function of wavelength. In order to specify the angles of incidence and reflection, it is necessary to know the directions of the sources, the direction of the sensor, and the direction of the normal to the target surface at the point in question. The direction of the sensor is an assigned parameter. The target surface normal can be

defined based on a combinatorial geometry algorithm developed by Armament Systems, Inc.[1*] This report describes an initial approach to modeling the direction, intensity, and spectral characteristics of each of the relevant sources of irradiation.

The model described here is a first approximation to a final model that will be used to predict the characteristics of naturally occurring radiation incident on a target. The work described here represents the status of this portion of the Ground Target Signature program six months after the inception of the program.

II. PROBLEM DESCRIPTION

The effort described in this report is the first step in predicting the characteristics of radiation incident on a ground target. In order to simplify the process at this stage, several limiting features were incorporated into the model. First, the wavelengths being considered in this report extend from 0.4 to 1.7 microns in 0.05 micron steps. This region was selected since it is of greatest concern at the present time, and since limited validation could be performed in the visual spectral region with equipment already on hand. Second, the situations being considered in this report limit the input to those from the sun and the cloudless daytime sky. The elimination of clouds from the problem precludes the immediate need to mathematically describe a cloud and simplifies correction and validation of the preliminary model. Third, radiation incident on the target after reflection from the ground is not being considered at this time since its effect is much less than that of the sun or sky. Also, except for very simple terrestrial configurations, the amount and distribution of radiation from this source would be much more difficult to model. Once a basic model has been generated and validated, these perturbing influeces can be added separately to create a more general model that can be applied for any set of precisely defined atmospheric and terrestrial conditions.

**References are listed on page 32.*

The model described in this report predicts the spectral irradiance (watts/cm^2 in a 0.05 micron band) reaching the ground from the sun and the clear daytime sky. The solar input is the solar irradiance outside the atmosphere multipled by the atmospheric transmission to the ground. The spectral irradiance produced by a defined segment of sky is determined through the format indicated in Figure 1.

A direct solar ray of irradiance H_s enters the atmosphere, and a fraction T_1 of this irradiance reaches a volume element within the field of view of a ground-based sensor. A certain fraction of the radiation will be scattered within this element. The amount of energy scattered within the element and the manner in which the scattered radiation is distributed in space are determined from the total and directional volume scattering functions. The radiation scattered within the cone Ω is then attenuated along the path to the ground. The transmission along this leg is T_2.

The total power arriving at the sensor, assumed for convenience to have an area of one square centimeter, in the wavelength band $\Delta\lambda$ is the sum of the contributions from all volume elements within the field of view. The result is

$$H = H_s \int_{r=o}^{r=\infty} B(\delta)\Omega T_1 T_2 dV \ , \qquad (1)$$

where r is the distance from the sensor to the scattering volume. H_s can be removed from the integral since it has no r dependence. This equation is strictly valid only for single scattering. Multiple scattering occurs when the sky, in addition to the sun, is a source of radiation which can be scattered into the field of view. It is of particular importance at short wavelengths where the scattering efficiency is high. The effect of multiple scattering will be addressed later in the program. The next section will be devoted to determining analytical expressions in terms of r for the various terms in equation (1) based on physical, geometric, and environmental parameters.

III. EVALUATION OF MODEL INPUT VARIABLES

A. Evaluation of H_s

H_s is determined by an integration of the Planck radiation equation and can be expressed as

$$H_s(\text{watts/cm}^2 \text{ in } \Delta\lambda) = \pi(\text{sr}) \times N(\text{watts/cm}^2\text{-sr}) \times D(\text{fraction of } N \text{ in } \Delta\lambda). \quad (2)$$

The quantity πN is a direct function of solar temperature (5750 degrees K), solar radius (6.956×10^{10} cm), and solar distance (1.495×10^{13} cm). The emitted solar irradiance is taken[2] as 6.211×10^3 watts/cm^2. The use of this value results in πN=0.1344 watts/cm^2. This quantity is the solar constant, and is usually given in units of calories/cm^2-min. Other references give its value as 0.1350,[3] 0.1393 ± 0.0028,[4] and 0.1392[5] watts/cm^2. For calculations in this report we will use the value πN = 0.139 watts/cm^2.

The fraction of this irradiance in various wavelength bands is given by

$$D = \left[\int_0^{\lambda+\Delta\lambda} N_\lambda d\lambda - \int_0^{\lambda} N_\lambda d\lambda \right] \Big/ \int_0^{\infty} N_\lambda d\lambda, \quad (3)$$

where N_λ (watts cm^{-2} sr^{-1} micron^{-1}) is the spectral radiance. The integral ratios given in equation (3) are tabulated in Reference 2. By assigning values to λ (0.40, 0.45, 0.50, etc., microns) and $\Delta\lambda$ (0.05 microns), we can determine H_s, as tabulated in Table I. These results are also shown in Figure 2 to provide a more graphic description of the wavelength dependence of the function.

B. Evaluation of ΩdV

Both Ω and dV can be determined from geometric parameters. The value of Ω is approximated by A/r^2, where A is the area of the sensor. Since we are assuming a sensor area of 1 cm^2, $\Omega = r^{-2}$. The scattering volume is given by $dV = \pi r^2 \tan^2 \frac{\alpha}{2} dr$, where α is the sensor field of view. The product ΩdV is then given by $\pi \tan^2 \frac{\alpha}{2} dr$. The final expression

is

$$\Omega dV = 10^{-5} \pi \tan^2 \frac{\alpha}{2} dr, \tag{4}$$

where dr is now expressed in kilometers.

C. Evaluation of B(δ)

The directional scattering efficiency B(δ) is a measure of the efficiency with which the incident irradiance is scattered into the sensor direction by 1 cm^3 of dV. It is a function of wavelength, the scattering angle, and r, since the number of scattering particles per cubic centimeter decreases with altitude. Two expressions for B(δ) are required, since radiation can be scattered either by Rayleigh or Mie particles.

The first step in determining B(δ) is calculating δ as a function of the geometric parameters. The expression which results is

$$\cos \delta = \cos \theta_s \cos \theta_L \cos \phi + \sin \theta_L \sin \theta_s, \tag{5}$$

where θ_s and θ_L are the elevation angles of the sun and the sensor field of view respectively, and ϕ is the azimuthal angle between them. These angles are specified as input parameters. The elevation and azimuthal angles of the sun can be found in standard references.[6] equation (5) is plotted in Figures 3 to 6 for various values of θ_s, θ_L, and ϕ.

Raleigh scattering, which is a special case of Mie scattering, occurs when electromagnetic radiation impinges on particles that are significantly smaller than the wavelength of the radiation. In this problem the Rayleigh particles of importance are air molecules. For unpolarized incident radiation, the equation describing the Rayleigh scattering is[7]

$$\beta(\delta)_R = \frac{2\pi^2(n-1)^2}{N\lambda^4}(1 + \cos^2\delta) \quad , \tag{6}$$

where n is the index of refraction of air and N is the number of molecules per cm^3. The wavelength dependent portion of this expression is $\frac{(n-1)^2}{\lambda^4}$, which is given for standard temperature and pressure as a function of wavelength in Table 1. This information was extracted from Reference 7 which cited Kuiper.[8] N can be shown to be 2.67×10^{19} molecules per cm^3 at zero degrees centigrade and pressure of 1013 millibars.

The altitude dependence of $\beta(\delta)$ is determined from ideal gas laws assuming an isothermal atmosphere. Both n-1 and N decrease with altitude as $e^{-h/8}$, where h is the altitude in kilometers.[7] The scale height of the Rayleigh atmosphere is 8 km, which is the altitude at which the density of the atmosphere drops to one third its sea level value. It is also the total height the Rayleigh atmosphere would have if it were all at sea level density. Our final expression is therefore

$$B(\delta)_R = \frac{2\pi^2 \times 10^5 (n_o-1)^2}{N_o \lambda^4}(1 + \cos^2\delta)\, e^{-r(\sin\theta_L)/8} \text{ km}^{-1} \text{ sr}^{-1}. \tag{7}$$

The subscript R indicates that it is the Rayleigh component of $B(\delta)$; the subscript o indicates sea level values of these quantities. The only δ dependence arises through the term $1 + \cos^2\delta$. Therefore, there is a two-to-one difference between the maximum and minimum directional scattering efficiencies in a Rayleigh medium. This will be seen to contrast sharply with the properties of Mie scattering that will be discussed next.

Mie scattering occurs when radiation impinges on particles whose radius is greater than or equivalent to the wavelength of the radiation. The total Mie scattering coefficient is given by[7]

$$\beta_{T,M} = \sum_{R=0}^{\infty} \pi \eta_R R^2 K_R \quad . \tag{8}$$

In this equation it is assumed that the droplets are spherical. This is a good assumption for droplets comprising haze or fog. η_R is the number of droplets per cubic centimeter with radii between R and R+dR, and K_R is the scattering area ratio which is a single-valued function of $2\pi R/\lambda$. K_R, which was first given by Houghton and Chalker,[9] is shown without fine structure in Figure 7. Physically, K_R is the ratio between the optical scattering cross section and the geometric cross section of a particle. Dessens[10] has estimated that the mean value of R in continental hazes is 0.4 micron for a high (~ 78 percent) relative humidity. If we assume that all droplets have this radius and that the total Mie coefficient can be converted to a directional Mie coefficient by introducing a function of δ, equation (8) becomes:

$$\beta(\delta)_M = 5.03 \times 10^{-4} \eta K_R f(\delta) \text{ km}^{-1} \text{ sr}^{-1} \quad . \tag{9}$$

K_R is given in Table I as a function of λ for R = 0.4 micron.

η can be inferred from the horizontal visibility V through the following procedure. The total scattering coefficient for a predominantly scattering atmosphere is given by $\beta = 3.912/V$ [11], where β is the sum of the Rayleigh and Mie total scattering coefficients in the visual region. The total Mie coefficient $\beta_{T,M,O} = 5.03 \times 10^{-4} \eta K_R \text{ km}^{-1}$. The total Rayleigh coefficient can be found by integrating equation (6) over the complete sphere resulting in

$$\beta_{T,R,O} = \int_{4\pi \text{ steradians}} \frac{2\pi^2(n-1)^2}{N\lambda^4} (1 + \cos^2 \delta) \, d\Omega = \frac{32\pi^3(n-1)^2 \times 10^5}{3N\lambda^4} \text{ km}^{-1} \tag{10}$$

This coefficient is listed in Table I as a function of λ for the visual portion of the spectrum.

The value of $\beta_{T,M,0}$ can now be expressed as

$$\beta_{T,M,0} = \sum_{\lambda=0.4}^{0.7} g_\lambda \left(\frac{3.912}{V} - \beta_{T,R,0} \right) \qquad (11)$$

for the visual portion of the spectrum. The function g_λ is a weighting factor representing the wavelength response of the human eye. The eye response is shown in Figure 8 plotted from data given in Reference 2. The curve was normalized to unit area, and the fractional areas in 0.05 micron steps were determined. These values of g_λ are given in Table I. A visibility can be assigned resulting in a value of $\beta_{T,M,0}$ from equation (11). When combined with K_R in equation (8), $\eta = \eta(V)$ can be determined with the results plotted in Figure 9.

This procedure can now be applied for other wavelengths. A value of V is assigned to determine η and a wavelength is assigned to determine K_R. Then $\beta_{T,M}$ is $5.03 \times 10^{-4}\ \eta\ K_R\ km^{-1}$. The results are shown in Figure 10.

The angular distribution of the Mie scattered radiation can be determined as follows. The total power in $\Delta\lambda$ scattered from one cubic centimeter of Mie particles is $H_s\ \beta_{T,M} \times 10^{-5}$ watts. The angular distribution of this power is given by curves found in several places in the technical literature.[11,12] The form used in this report was taken from Deirmendjian.[13] These data were plotted as $f(\delta)$ in Figure 11 after normalization such that

$$\int_{4\pi \text{ steradians}} f(\delta)\, d\Omega = 1 \quad .$$

The variation of $\beta_{T,M} + \beta_{T,R}$ with a altitude is indicated by Middleton[11], citing Waldram.[14] The curves are shown in Figure 12. The letters assigned to some of these curves will be discussed in the next section. It can be seen that there are large differences between the various curves. On the average, the Mie volume scattering coefficient varies with altitude as $e^{-h/4.1\ km}$ for h ≥ one kilometer; however, it should be noted that for high ground level values of $\beta_{T,M}$ the rate of decrease of $\beta_{T,M}$ with altitude is much more rapid at the lower altitude than at the higher altitudes. The model used to approximate these curves will be discussed in more detail in the next section, but briefly the situation is as follows. If β_T is small [$V \geq G(\lambda)$], the altitude variation goes as $\beta_{T,M} = \beta_{T,M,O}\ e^{-h/4.1km.}$ If $V < G(\lambda)$, the curves are approximated by two line segments such that the scale height is 4.1 kilometers for h ≥ 1 km and a kilometers for h < 1 km. We will now determine values for $G(\lambda)$ and a.

$G(\lambda)$ can be determined by specifying the value of $\beta_{T,M}$ at some altitude. This specification was made somewhat arbitrarily by an assumption that $\beta_{T,M,\text{visual region}} \leq 0.1\ km^{-1}$ at an altitude of one km. The curve passing through the $\beta_{T,M} = 0.1\ km^{-1}$, h = 1 km point, with a scale height of 4.1 km, reaches the zero altitude line at $\beta_{T,M} = 0.128\ km^{-1}$. The visibility represented by $\beta_{T,M,\text{visual region}} = 0.128\ km^{-1}$ is designated $G(\lambda)$ and can be found by replotting Figure 10. The result is shown in Figure 13.

The scale height of the lower atmosphere, a, can be determined by finding the equation of the exponential curve connecting the points

$$\beta_{T,M} = \sum_{\lambda=0.4}^{0.7} 5.03 \times 10^{-4}\ \eta K_R g_\lambda,\ h = 0) \text{ and } (\beta_{T,M} = 0.1\ km^{-1},\ h = 1\ km).$$

The result is $a = -1/\ln\ (0.1/\beta_{T,M,O})$, where $\beta_{T,M,O}$ is the Mie volume

scattering coefficient at ground level shown in Figure 10. After substituting $h = r \sin \theta_L$, the following expressions can be applied directly.

$$\text{If } V \geq G(\lambda),\ \beta_{T,M} = \beta_{T,M,O}\, e^{-(r \sin \theta_L)/4.1} \quad 0 < r < \infty \ . \tag{12}$$

$$\text{If } V < G(\lambda),\begin{cases} \beta_{T,M} = \beta_{T,M,O}\, e^{\,r \sin \theta_L \ln(0.1/\beta_{T,M,O})} & 0 < r < 1/\sin \theta_L, \\ \beta_{T,M} = 0.128\, e^{-(r \sin \theta_L)/4.1} & 1/\sin \theta_L < r < \infty \ , \end{cases}$$

where $\beta_{T,M,O} = 5.03 \times 10^{-4}\, \eta\, K_R$. The directional Mie scattering coefficient is then given by

$$B(\delta)_M = 5.03 \times 10^{-4}\, \eta\, K_R\, f(\delta)\, B(r) \ , \tag{13}$$

where

$$\text{if } V \geq G(\lambda),\ B(r) = e^{-(r \sin \theta_L)/4.1} \qquad 0 < r < \infty$$

$$\text{if } V < G(\lambda),\begin{cases} B(r) = e^{\,r \sin \theta_L \ln(0.1/\beta_{T,M,O})} & 0 < r < 1/\sin \theta_L \\ B(r) = e^{-(r \sin \theta_L)/4.1} & 1/\sin \theta_L < r < \infty \end{cases} \tag{14}$$

D. Evaluation of $T_1\ T_2$

The transmission over the two-legged path (Figure 1) is the product of four individual transmissions. The transmissions through the Rayleigh and Mie scattering components have already been mentioned. There is, however, also absorption by water vapor and carbon dioxide, which will be discussed using the geometry shown in Figure 14.

The horizontal transmission by the Rayleigh component of the atmosphere is $T_{r'} = \exp(-r' \beta_{T,R})$. However, for slant paths, $\beta_{T,R}$ is a

function of r' so we must evaluate the expression $T_r = \exp\left[-\int_o^r B(r')dr'\right]$.

To determine the form of B(r') we must integrate equation (7, with respect to $d\Omega$ over all directions. The result is

$$B_{T,R}(r') = \frac{32\pi^3 (n-1)^2 \times 10^5}{3N\lambda^4} e^{-(r' \sin \theta_L)/8} \text{ km}^{-1}. \qquad (15,$$

When this value is substituted into the transmission equation using the geometry of Figure 14, the result is

$$T_{r'} = \left\{\exp\left[-\int_o^r \beta_{T,R,0}\, e^{-(r' \sin \theta_L)/8}\, dr'\right]\right\} \times \left\{\exp\left[-\int_o^\infty \beta_{T,R,0}\, e^{-(r \sin \theta_L + R \sin \theta_S)/8}\, dR\right]\right\}. \qquad (16)$$

When the integrations are performed and the r dependence is factored out, the resulting expression is

$$T_{r'} = \left\{\exp\left[\frac{-8\beta_{T,R,0}}{\sin \theta_L}\right]\right\} \times \left\{\exp\left[-8\beta_{T,R,0}\left(\frac{1}{\sin \theta_S} - \frac{1}{\sin \theta_L}\right) e^{-(r \sin \theta_L)/8}\right]\right\}, \qquad (17)$$

where $\beta_{T,R,0}$ is given by equation (10).

The absorbing components of the atmosphere behave in a different manner from the scattering components. For convenience, we will define a distance which contains the same amount of absorbing material as the

total light path. This distance will be called the optical slant range.

The carbon dioxide optical slant range will be given the symbol ρ. It will be assumed here that since carbon dioxide is a permanent atmospheric gas its concentration will decrease with altitude at the same rate as the Rayleigh component. Thus, using the geometry of Figure 14,

$$\rho = \int_0^r e^{-(r' \sin \theta_L)/8} \, dr' + \int_0^\infty e^{-(r \sin \theta_L + R \sin \theta_S)/8} \, dR \, . \qquad (18)$$

When the integrations are performed and the r dependence is factored out, the resulting expression is

$$\rho = \frac{8}{\sin \theta_L} + 8\left(\frac{1}{\sin \theta_S} - \frac{1}{\sin \theta_L}\right) e^{-(r \sin \theta_L)/8} \text{ km} \, . \qquad (19)$$

This equation is plotted in Figures 15, 16, and 17. Several features of these graphs are readily apparent, as listed below.

(1) When $\theta_L = \theta_S$, ρ is dependent on r.

(2) When $\theta_L < \theta_S$, ρ increases with increasing r.

(3) When $\theta_L > \theta_S$, ρ decreases with increasing r.

(4) $\rho_{max} = \frac{8}{\sin \theta_S}$ or $\frac{8}{\sin \theta_L}$, whichever is greater.

(5) $\rho_{min} = 8$ kilometers, the CO_2 atmospheric optical depth.

It has been demonstrated[15,16] that carbon dioxide absorption can be described by an error function absorption law, namely

$$T_c = 1 - \text{erf } K(\lambda) \sqrt{\rho}, \quad \text{where erf } Z = \frac{2}{\sqrt{\pi}} \int_0^z e^{-t^2} \, dt \, . \qquad (20)$$

$K(\lambda)$ as used in this study was determined by plotting transmission data given in Hackforth,[15] integrating under the curve in 0.05 micron bands, and converting the results to obtain a value of $K(\lambda)$ for that band.

The error function can be expanded in an infinite series as

$$\text{erf } Z = \frac{2Z}{\sqrt{\pi}} \left[1 - \frac{Z^2}{3} + \frac{Z^4}{10} - \ldots + \frac{(-1)^n Z^{2n}}{(2n+1)\, n!} + \ldots\right] . \quad (21)$$

The maximum value of $K(\lambda)$ in the 0.4 to 1.7 micron interval is 0.0075. The maximum value of ρ will be taken as $8/\sin 10^\circ = 46.07$.

Thus $Z_{max} = 0.0075 \sqrt{46.07} = 0.0509$. Therefore,

$$\text{erf } Z_{max} = \frac{2 \times 0.0509}{\sqrt{\pi}} \left[1 - \frac{0.00259}{3} + \frac{0.0000067}{10} - \ldots.\right] . \quad (22)$$

Obviously, the second and succeeding terms can be ignored; thus our final expression for carbon dioxide transmission is

$$T_C = 1 - \frac{2}{\sqrt{\pi}} K(\lambda) \sqrt{\rho} = 1 - \alpha(\lambda)\sqrt{\rho} , \quad (23)$$

where ρ is given by equation (19). The values of $\alpha(\lambda)$ are given in Table I.

Absorption by water vapor follows a similar law, namely,[15]

$$T_H = 1 - \text{erf } \frac{\beta(\lambda)}{2} \sqrt{\pi W} , \quad (24)$$

where $\beta(\lambda)$ is the water vapor error function absorption coefficient and W is the number of centimeters of precipitable water vapor in the light path. The distribution of water vapor with altitude can be found on a graph[5] relating the altitude and the mixing ratio (grams of water per kilogram of dry air) for a ground level humidity of 7.35 grams of water per cubic meter of dry air. This curve was altered to represent W^* (cm of precipitable water vapor per km of horizontal path) as a function of altitude. The results are shown in Figure 18.

It can be seen that on the logarithmic plot the low altitude portion of the curve can be approximated by a straight line equivalent to

$$W^* = W_o^* \, e^{-h/2} \quad , \tag{25}$$

where W_o^*, the ground level value of W^*, is a function of temperature and relative humidity as shown in Figure 19.

W can be determined using the geometry of Figure 14. Thus,

$$W = \int_o^r W_o^* \, e^{-(r' \sin \theta_L)/2} \, dr' + \int_o^\infty W_o^* \, e^{-(r \sin \theta_L + R \sin \theta_S)/2} \, dR \quad . \tag{26}$$

When the integrations are performed and the r dependence is removed, the result is

$$W = \frac{2W_o^*}{\sin \theta_L} + 2W_o^* \left(\frac{1}{\sin \theta_S} - \frac{1}{\sin \theta_L}\right) e^{-(r \sin \theta_L)/2} \quad . \tag{27}$$

This equation is plotted in Figures 20, 21 and 22. Again, several features of these graphs are readily apparent:

(1) When $\theta_L = \theta_S$, W is independent of range.

(2) When $\theta_L < \theta_S$, W increases with increasing range.

(3) When $\theta_L > \theta_S$, W decreases with increasing range.

(4) $W_{max} = \frac{2W_o^*}{\sin \theta_S}$ or $\frac{2W_o^*}{\sin \theta_L}$, whichever is greater.

(5) $W_{min} = 2W_o^*$, the water vapor atmospheric optical depth.

The absorption coefficient was determined by integrating transmission data given in Hackforth.[15] The maximum value was found to be 1.264. The maximum value of W will be taken as $\frac{2 \times 10}{\sin 10^{o}} = 116.3$.

Thus $Z_{max} = 0.632 \sqrt{116.3\pi} = 12.1$. Since the error function series expansion converges very slowly for this value of Z, a rational approximation to erf Z was found[17,18] for ease in programming the equation. This approximation states:

$$T_H = 1 - \text{erf } Z = \left[\frac{0.34802}{(1+0.47047Z)} - \frac{0.09588}{(1+0.47047Z)^2} + \frac{0.74786}{(1+0.47047Z)^3}\right] e^{-Z^2} + \varepsilon(Z) \,, \tag{28}$$

where $|\varepsilon(Z)| \leq 2.5\times10^{-5}$ and $Z = \frac{\beta(\lambda)}{2} \sqrt{\pi W} = \gamma(\lambda) \sqrt{W}$. $\gamma(\lambda)$ is given in Table I.

The transmission through the Mie scattering component again requires separation on the basis of the ground level visibility. If $V \geq G(\lambda)$, we can use equation (12) and the geometry of Figure 14. The result is

$$T_M = \exp -\left\{\int_0^r \beta_{T,M,0}\, e^{-(r' \sin \theta_L)/4.1}\, dr'\right\} \times \exp -\left\{\int_0^\infty \beta_{T,M,0}\, e^{-(r \sin \theta_L + R \sin \theta_S)/4.1}\, dR\right\} . \tag{29}$$

This expression reduces to

$$T_M = \exp\left\{\frac{-4.1\ \beta_{T,M,0}}{\sin \theta_L}\right\} \times \exp\left\{-4.1\ \beta_{T,M,0} \left(\frac{1}{\sin \theta_S} - \frac{1}{\sin \theta_L}\right) e^{-(r \sin \theta_L)/4.1}\right\} . \tag{30}$$

If $V < G(\lambda)$, we must distinguish between the cases where $r < 1/\sin\theta_L$ and $r > 1/\sin\theta_L$. The geometries associated with these cases are shown in Figures 23 and 24. The values of $\beta_{T,M}$ for each segment are also indicated on these Figures. When $r < 1/\sin\theta_L$ (Figure 23),

$$T_M = \exp\left\{-\int_{\frac{1}{\sin\theta_S}}^{\infty} 0.128\, e^{-(R\sin\theta_S)/4.1}\, dR\right\} \times \exp\left\{-\int_{\frac{r\sin\theta_L}{\sin\theta_S}}^{\frac{1}{\sin\theta_S}} \beta\, e^{R\sin\theta_S \ln(0.1/\beta)}\, dR\right\} \times \exp\left\{-\int_{0}^{r} \beta\, e^{r'\sin\theta_L \ln(0.1/\beta)}\, dr'\right\}, \quad (31)$$

where $\beta_{T,M,O}$ is given the symbol β. This expression reduces to

$$T_M = \exp\left\{\frac{\beta/\ln(0.1/\beta)}{\sin\theta_L} - \frac{0.1/\ln(0.1/\beta) + 0.41}{\sin\theta_S}\right\} \times \exp\left\{\frac{\beta}{\ln(0.1/\beta)}\left[\frac{1}{\sin\theta_S} - \frac{1}{\sin\theta_L}\right] e^{r\sin\theta_L \ln(0.1/\beta)}\right\}. \quad (32)$$

When $r > 1/\sin\theta_L$ (Figure 24),

$$T_M = \exp\left\{-\int_{\frac{r\sin\theta_L}{\sin\theta_S}}^{\infty} 0.128\, e^{-(R\sin\theta_S)/4.1}\, dR\right\} \times \exp\left\{-\int_{\frac{1}{\sin\theta_L}}^{r} 0.128\, e^{-(r'\sin\theta_L)/4.1}\, dr'\right\} \times \exp\left\{-\int_{0}^{\frac{1}{\sin\theta_L}} e^{r'\sin\theta_L \ln(0.1/\beta)}\, dr'\right\}. \quad (33)$$

This expression reduces to

$$T_M = \exp\left\{\frac{(\beta-0.1)/\ln(0.1/\beta) - 0.41}{\sin\theta_L}\right\} \times \exp\left\{-0.51\left[\frac{1}{\sin\theta_S} - \frac{1}{\sin\theta_L}\right] e^{-(\sin\theta_L)/4.1}\right\} . \quad (34)$$

These expressions can be checked in part by evaluation at the limits of applicability. If equations (32) and (34) are evaluated at the point $r = 1/\sin\theta_L$, they are identical expressions, namely,

$$T_M = \exp\left\{\frac{(\beta-0.1)/\ln(0.1/\beta)}{\sin\theta_L} - \frac{0.41}{\sin\theta_S}\right\} . \quad (35)$$

If $r = 1/\sin\theta_L$ is substituted into equation (30) and equations (30) and (35) are solved at the limit $V = G(\lambda)$ ($\beta = 0.128$), identical expressions result, namely,

$$T_M = \exp\left\{\frac{-0.11}{\sin\theta_L} - \frac{0.41}{\sin\theta_S}\right\} . \quad (36)$$

One other check is available. If we let $\theta_L = \theta_S = 90$ degrees in equation (36), we should arrive at the same solution as the horizontal transmission solution of $T_M = \exp(-R\beta)$, where $R = 4.1$ km (the Mie scattering scale height for $V = G(\lambda)$ and $\beta = 0.128$). This also is found to check, resulting in $T_M = 0.59$.

IV. UTILIZATION OF THE MODEL

As shown in Section II, the problem can be reduced to the evaluation of an integral containing several r-dependent variables over all values of r. The integral in its most usable form is obtained by rewriting equation (1) as

$$H = H_S \int_{r=0}^{r=\infty} B(\delta)\Omega T_R T_M T_C T_H \, dV \quad . \tag{37}$$

Each of these variables has been evaluated as a function of r and λ earlier in this report. For convenience, the location of each will now be summarized. H_S is given in Table I. The geometric variable ΩdV is given by equation (4). $B(\delta)$ is the sum of the components from Rayleigh and Mie scattering. The Rayleigh component is described by equation (7) where $N_o = 2.67 \times 10^{19}$, $(n_o-1)^2/\lambda^4$ is given in Table I, and δ can be determined from equation (5). The Mie component is described by equation (13) where η is given in Figure 9, K_R is given in Table I, $f(\delta)$ is shown in Figure 11, and $B(r)$ is given by equations (14). $G(\lambda)$, the visibility parameter, is given in Figure 13.

The transmission requires four terms, since scattering by Rayleigh and Mie particles and absorption by carbon dioxide and water vapor must be taken into account. T_R is described by equation (17) where $\beta_{T,R,O}$ is given in equation (10). T_M is described by equations (30), (32) and (34) with $G(\lambda)$ again given by Figure 13. $\beta_{T,M,O}$ is defined as $5.03 \times 10^{-4} \eta K_R(\lambda)$. T_c is described by equation (20) with $\alpha(\lambda)$ given in Table I and ρ given by equation (19). T_H is given by equation (28) where $Z = \gamma(\lambda)\sqrt{W}$. $\gamma(\lambda)$ is given in Table I, W is given in equation (27), and W_o^* can be determined from Figure 19.

An upper limit of infinity cannot be handled by the computer; therefore, an upper limit was assigned based on the following procedure. The most slowly converging term in the integral is the Rayleigh

scattering term having a scale height of eight kilometers. We can therefore determine the value of b for which

$$\frac{\sin \theta_L}{8} \int_0^b e^{-r \sin \theta_L/8} \, dr = 0.999$$

and be assured that substitution of this value for the upper limit in equation (37) will result in an error in the value of the integral of less than 0.1 percent. This value of b is found to be $56/\sin \theta_L$.

These terms can be combined and simplified, resulting in an equation of the form

$$H = A \int_B^C \left\{De^{Fr} + Ge^{Hr}\right\} \left\{\exp\left[I + Je^{Hr}\right]\right\} \left\{\exp\left[Ke^{Fr}\right]\right\} \times$$

$$\left\{1 - L\sqrt{Me^{Fr} - 1/F}\right\} \left\{\left[\frac{0.34802}{(1+0.470472)} - \frac{0.09588}{(1+0.470472)^2} + \right.\right. \qquad (38)$$

$$\left.\left. \frac{0.74786}{(1+0.470472)^3}\right] \times e^{-Z^2}\right\} dr \ ,$$

where $A = H_S \tan^2 \frac{\alpha}{2} \exp\left[\frac{-9.9 \times 10^{-12} (n_o-1)^2/\lambda^4}{\sin \theta_L}\right]$, $D = 2.3 \times 10^{-18} \times (1+\cos^2\delta) (n_o-1)^2/\lambda^4$, $F = \sin \theta_L/8$, $G = 1.58 \times 10^{-8} \eta K_R f(\delta)$,

$K = 9.9 \times 10^{-12} (\csc \theta_S - \csc \theta_L) (n_o-1)^2/\lambda^4$, $L = \alpha(\lambda)$,

$M = 8(\csc \theta_S - \csc \theta_L)$, and

$$Z = \gamma(\lambda) \sqrt{\frac{2W_o^*}{\sin \theta_L} + 2W_o^* (\csc \theta_S - \csc \theta_L) e^{-r \sin \theta_L/2}} \ .$$

The remaining inputs are functions of $G(\lambda)$. If $V \geq G(\lambda)$, only one integral is required and $B = 0$, $C = 56/\sin\theta_L$, $H = -\sin\theta_L/4.1$, $I = -4.1\beta/\sin\theta_L$, and $J = -4.1\beta(\csc\theta_S - \csc\theta_L)$. If $V < G(\lambda)$, the required solution is the sum of two integrals. The first is represented by $B = 0$, $C = 1/\sin\theta_L$, $H = \sin\theta_L \ln(0.1/\beta)$,

$$I = \frac{\beta/\ln(0.1/\beta)}{\sin\theta_L} - \frac{0.1/\ln(0.1/\beta) + 0.41}{\sin\theta_S}, \text{ and}$$

$J = \beta(\csc\theta_S - \csc\theta_L)/\ln(0.1/\beta)$. The second integral is represented by $B = 1/\sin\theta_L$, $C = 56/\sin\theta_L$, $H = -\sin\theta_L/4.1$,

$I = \frac{(\beta-0.1)/\ln(0.1/\beta)-0.41}{\sin\theta_L}$, and $J = -0.51(\csc\theta_S - \csc\theta_L)$. The β which appears in these expressions is $\beta_{T,M,0}$ given by $5.03 \times 10^{-4}\, nK_R$.

In order to provide a limited validation of part of this model, a comparison was made between the transmission predicted by the model from the ground level visibility and that determined from actual values of the altitude dependence of the visual spectrum volume scattering coefficient. The Mie transmission predicted by the model is given by $T_M = \exp\left[-\int_0^H B_M(r)dr\right]$. The value of $B_M(r)$ for this expression is shown in Figure 25 as a function of the ground level visibility. When $V < G(\lambda)$, two curves are required. As V approaches $G(\lambda)$, the slope of the lower segment approaches that of the upper segment. At $V = G(\lambda)$ only one curve is required, and for further increase in V the entire curve is translated while keeping the same slope. The Mie transmission along one of these curves to an altitude of nine kilometers is found by letting θ_L equal 90 degrees and integrating equation (13) from $r = 0$ to $r = 9$ km. $\beta_{T,M,0}$ is given by equation (11). The Rayleigh transmission can be found by letting θ_L equal 90 degrees and integrating equation (15) from $r = 0$ to $r = 9$ km. The product of the Rayleigh

and Mie transmissions represents the total transmission over the vertical path to an altitude of nine kilometers as predicted by the model.

This procedure was applied to the curves labeled (a) through (f) in Figure 12. The individual curves were also approximated by a large (~20) number of straight line segments, the transmission over each segment was determined, and the product of the transmissions was found for each curve. The transmissions determined by the two methods were compared and errors of 3.9, 2.4, 1.2, 27.5, 0.8, and 10.5 percent were found for curves (a) through (f) respectively. The large error on curve (d) resulted from the increase in $\beta_{T,M}$ with altitude, which is not a common occurrence on a clear day.

V. CONCLUSIONS

An atmospheric radiative transfer model based on single scattering has been described in this report. At this stage it is not known how useful it is; however, certain features are clear. First, the geometry shown in Figure 1 is generally applicable to problems of this kind, provided multiple scattering can be ignored. Second, equation (1) fully describes the geometry in the figure, although defining the terms in the integral for non-ideal conditions will not generally be so straightforward as described here. Third, it is desirable to use a simple model of this nature, since at the time a data point is desired it is unlikely that detailed information about the scattering and absorbing properties of the upper atmosphere will be known. Thus, some measure of predictability based on measurements that can be made at ground level is required.

In the course of this program, several sources of error have been found. The errors tend to occur in three general classes. The first class of errors results from simplifications and approximations used to keep the model from being overly complicated. One such error results from the atmospheric transmission model being based on a flat earth assumption. The validity of this assumption is a strong function

of θ_L and θ_s. An analysis was made of this error source, and it was found that the error is less than one percent, provided that both θ_L and θ_s are greater than five degrees. Another error in this class results from the manner in which the Mie scattering coefficient is derived from the visibility. The Mie scattering coefficient used in the model is based on the number of droplets per cubic centimeter in the volume element. It is assumed, for convenience, that all droplets have the same radii, corresponding to a mean radius found in continental hazes. In reality, however, there is a spread in radius. The effect of this error is currently being analyzed.

The second class of error results from inadequate knowledge of some of the basic input parameters. Some of these uncertainties include the manner in which the concentrations of water vapor, carbon dioxide, and water droplets vary with altitude, and the way the mean droplet radius varies with the visibility. As better values for these parameters become available, the model can be easily modified to accommodate them.

The third class of error arises from basic limitations in the modeling process itself. Consider, as an example, the transmission of direct solar radiation. If we use best estimates of the manner in which the concentrations of scattering and absorbing particles vary with altitude, we can predict a vertical transmission which will be in error by some amount because of errors we described as class two. If now the sun is found to be in some direction other than vertical, this error will be amplified because of the greater atmospheric path the radiation traverses. For example, if our vertical transmission error is +10 percent, a solar elevation angle of 30 degrees results in an error of +21 percent and a solar elevation angle of 10 degrees results in an error of +74 percent.

Another problem with a model of this nature is that predictions of properties of the upper atmosphere are being made based on ground level measurements. This, of necessity, limits the cases in which

the model can be used. For example, if reflection occurs from temperature inversion boundaries, the model cannot be applied to cases in which an inversion layer exists.

Plans for the next six months include several phases. First, some limited validation measurements will be made in the visual portion of the spectrum, including luminance measurements of the sun and the clear daytime sky. These measurements will be converted to radiometric units and compared to predictions made with the model. The effect of multiple scattering will be addressed at this point.

Second, luminance measurements will be made of solar-irradiated armor plate. These measurements will be compared with predictions provided by the model after using available bidirectional reflectivity data.

Third, the error analysis will be continued in an attempt to define more accurately the conditions under which the model can be utilized.

Finally, the effect of the ground as a radiation source will be considered to determine those cases in which its effect may be ignored and those in which its inclusion is mandatory.

REFERENCES

1. "MAGIC Computer Simulations, Vol. II, Part I," Naval Weapons Center Technical Note No. 4566-3-71, Vol. II, May 1971.

2. Mark Pivovonsky and Max Nagel, Tables of Blackbody Radiation Functions, The Macmillan Co., 1961.

3. Wasley S. Krogdahl, The Astronomical Universe, The Macmillan Co., 1952.

4. Handbook of Chemistry and Physics - 40th Edition, Chemical Rubber Publishing Co., 1959.

5. William L. Wolfe, ed., Handbook of Military Infrared Technology, Office of Naval Research, Dept of the Navy, 1965.

6. Smithsonian Institution, Smithsonian Meteorological Tables - Sixth Revised Edition, Wash., DC, 1958.

7. Sperry Gyroscope Company Electro-Optics Group, Scattering - The Interaction of Light and Matter, Sperry Report No. AB-1272-0057, February 1966.

8. G. F. Kuiper, The Atmospheres of the Earth and Planets, University of Chicago Press, 1952.

9. H. G. Houghton and W. R. Chalker, "Scattering Cross Sections of Water Drops in Air for Visible Light," JOSA, Vol. 39, No. 11, November 1949.

10. H. Dessens, "Brume et Noyaux de Condensation," Ann. de Geophys., Vol. 3, 1947.

11. W. E. K. Middleton, Vision Through the Atmosphere, University of Toronto Press, 1958.

12. Max Born and Emil Wolf, Principles of Optics - Third Ed., Pergamon Press, 1964.

13. D. Deirmendjian, Electromagnetic Scattering on Spherical Polydispersions, American Elsevier Publishing Co., Inc., New York 1969.

14. J. M. Waldram, "Measurement of the Photopic Properties of the Upper Atmosphere," Trans. Illum. Eng. Society (London), Vol. 10, 1945.

REFERENCES (CONT.)

15. Henry L. Hackforth, Infrared Radiation, McGraw-Hill Book Company, Inc., 1960.

16. L. Larmore, "Transmission of Infrared Radiation Through the Atmosphere," Proc. IRIS - Vol.I, No. 1, June 1956.

17. C. Hastings, Jr., Approximations for Digital Computers, Princeton University Press, Princeton, NJ, 1955.

18. M. Abramowitz and I. A. Stegun, ed's., Handbook of Mathematical Functions, National Bureau of Standards, November 1967.

APPENDIX A

ILLUSTRATIONS

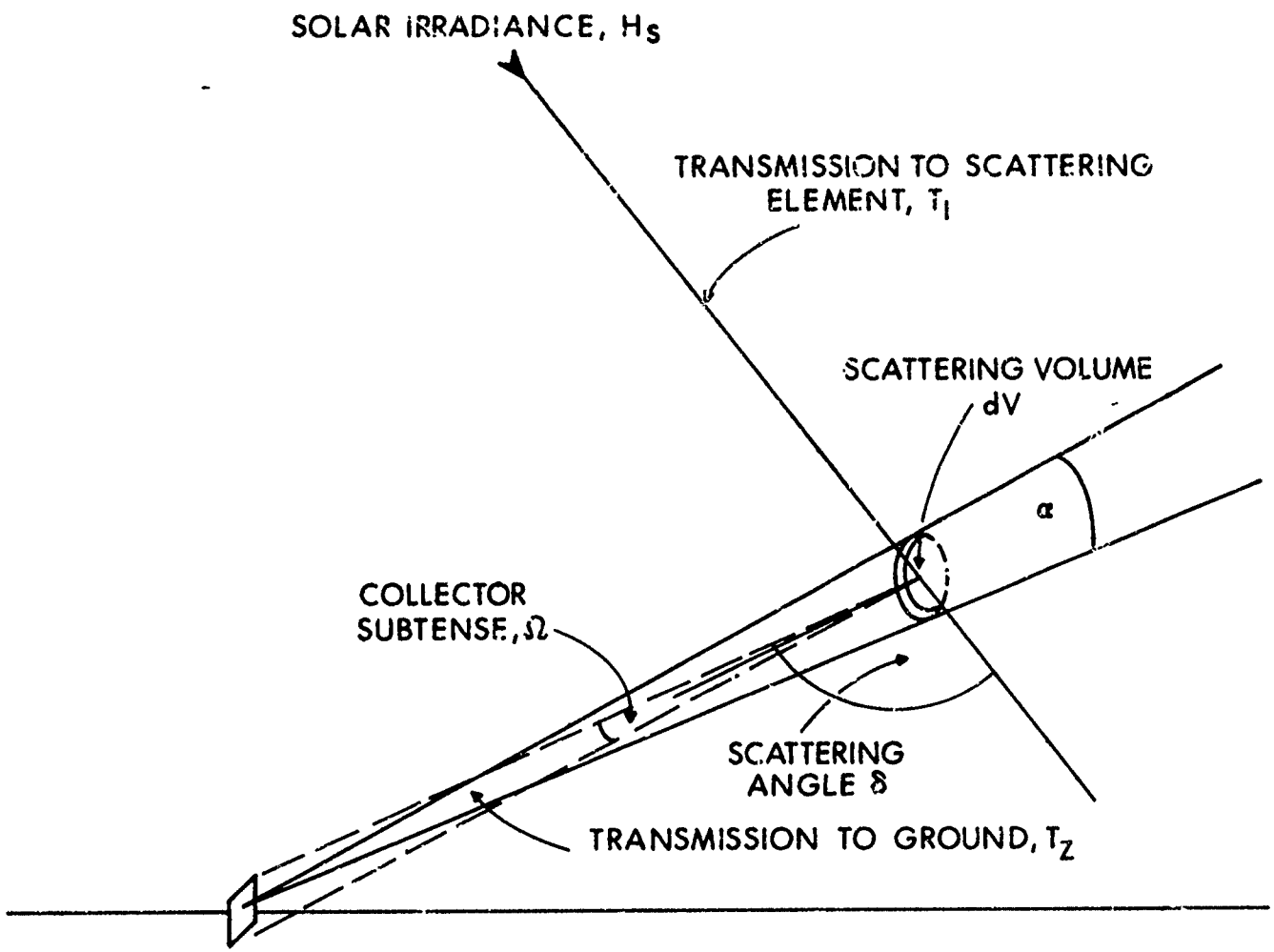

Figure 1. Format Used in Predicting Sky Radiance.

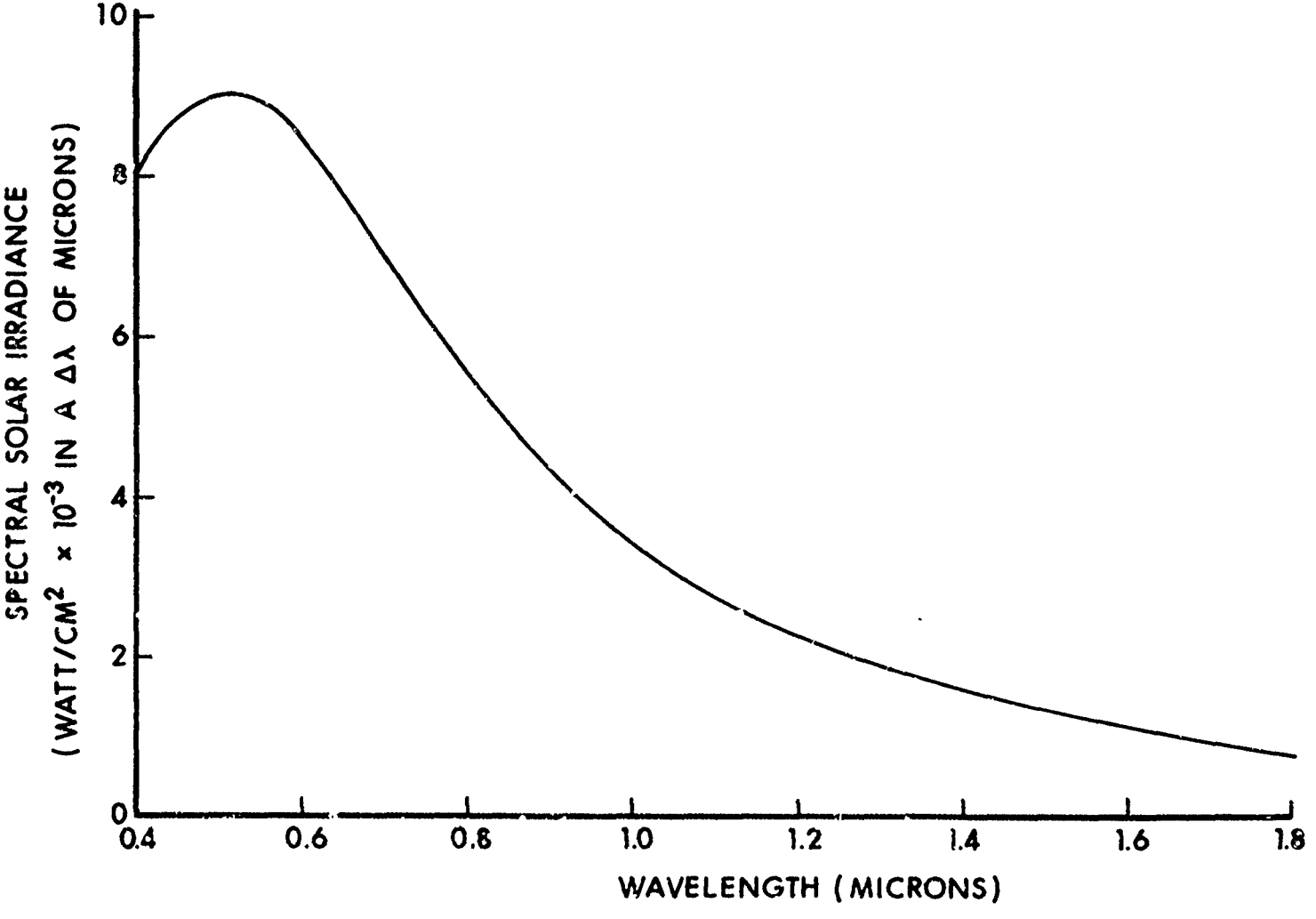

Figure 2. H_s as a Function of Wavelength.

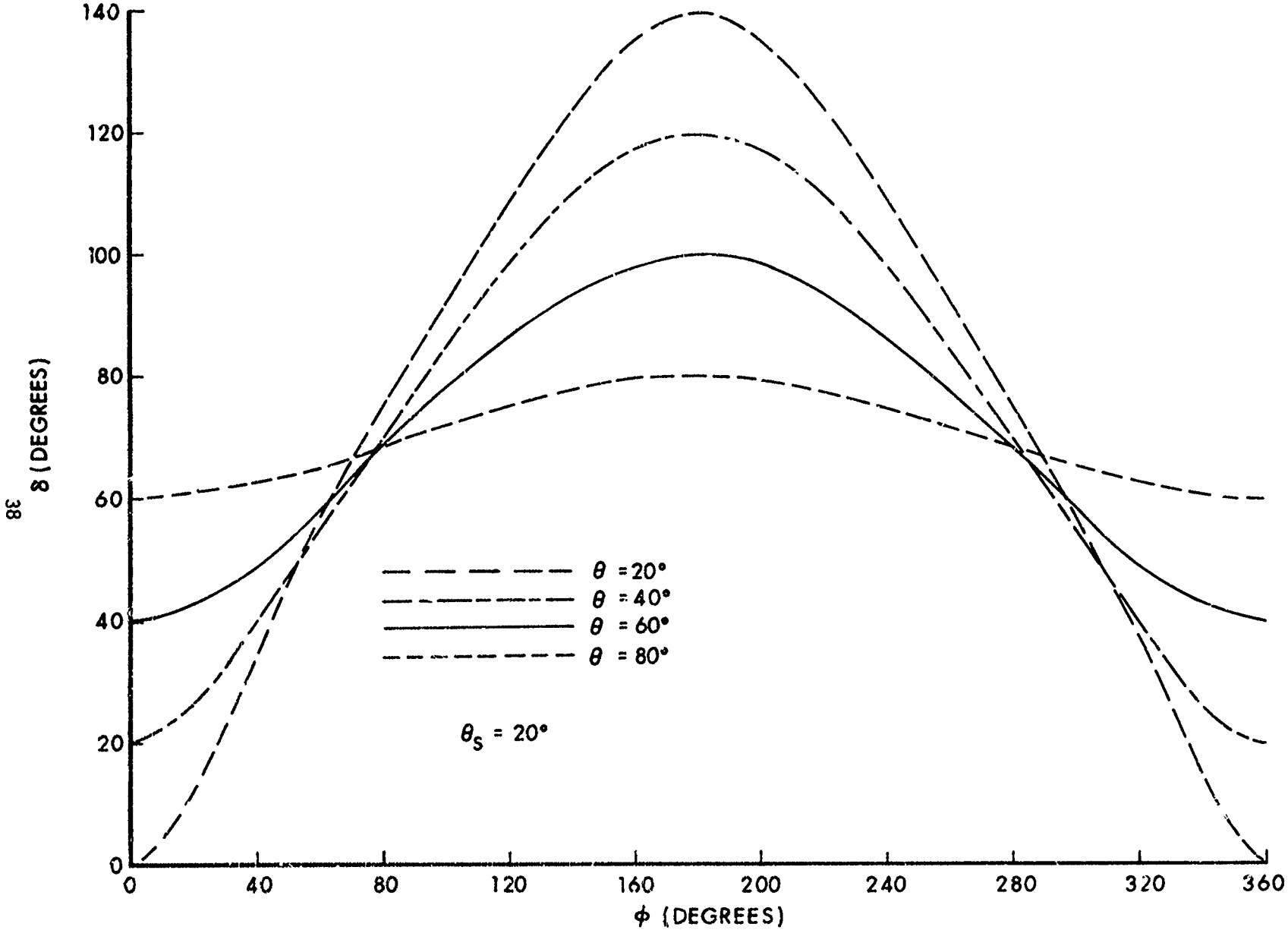

Figure 3. δ as a Function of θ_L and ϕ for θ_S = 20 Degrees.

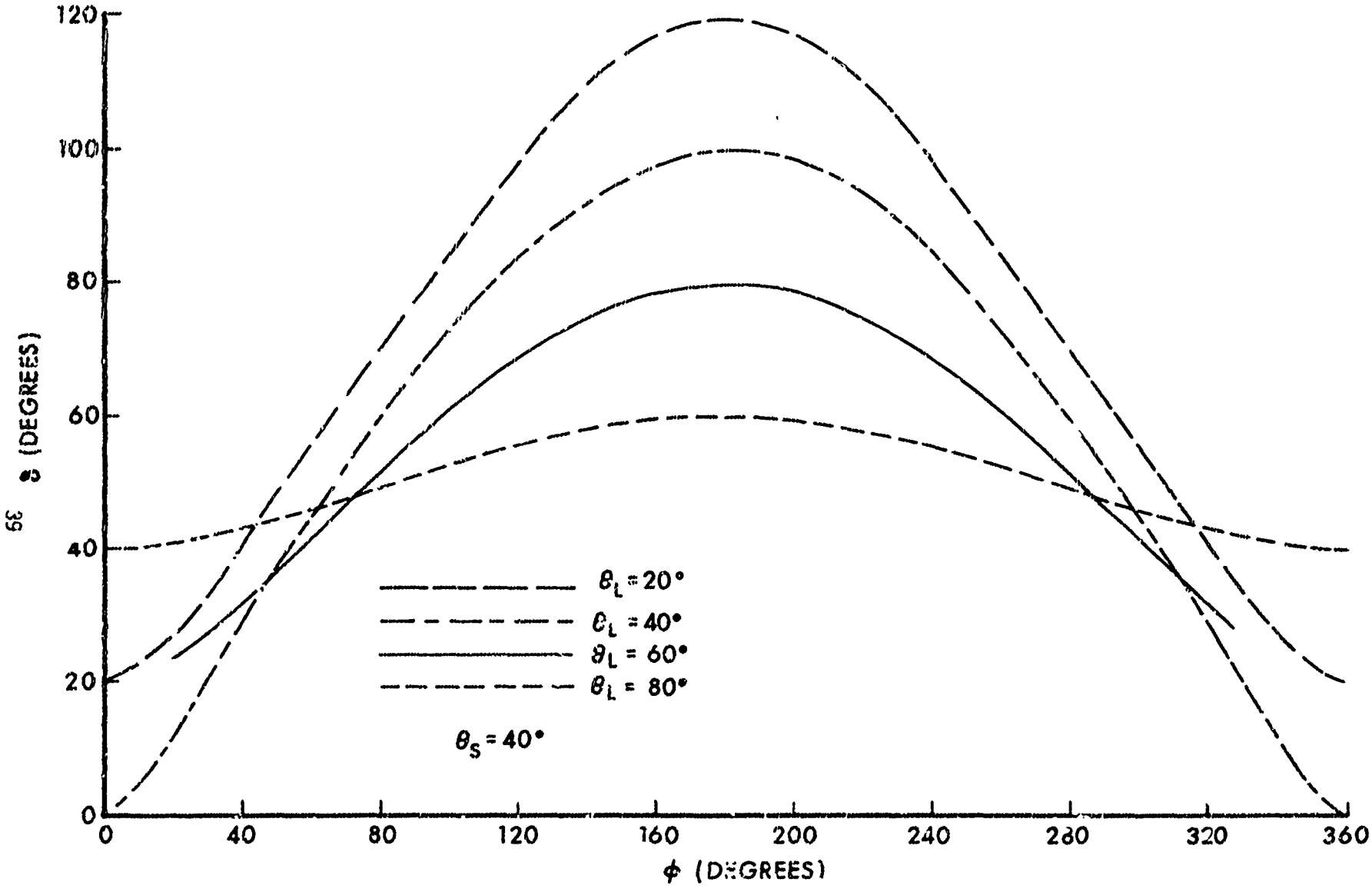

Figure 4. δ as a Function of θ_L and ϕ for θ_S = 40 Degrees.

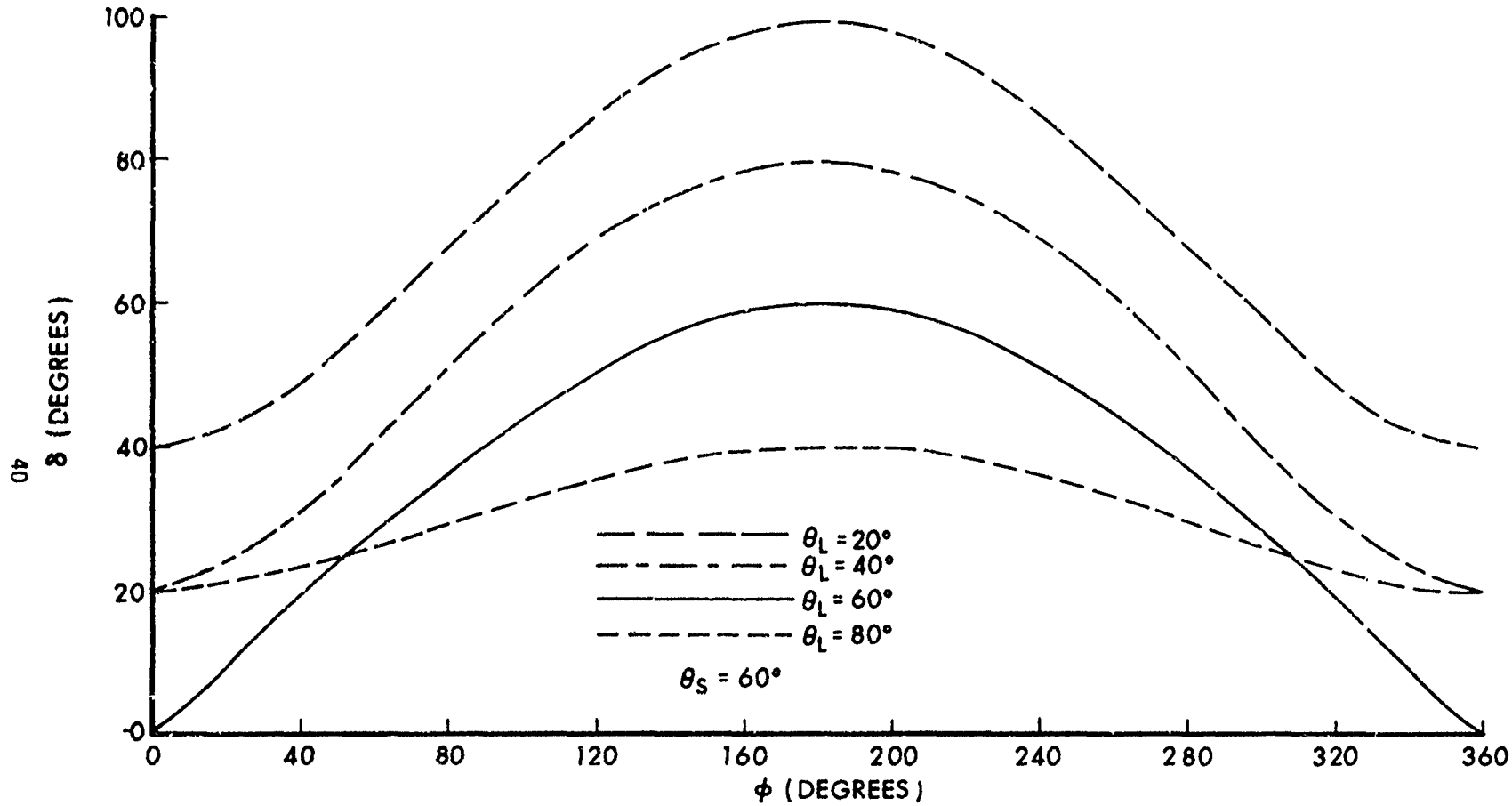

Figure 5. δ as a Function of θ_L and ϕ for θ_S = 60 Degrees.

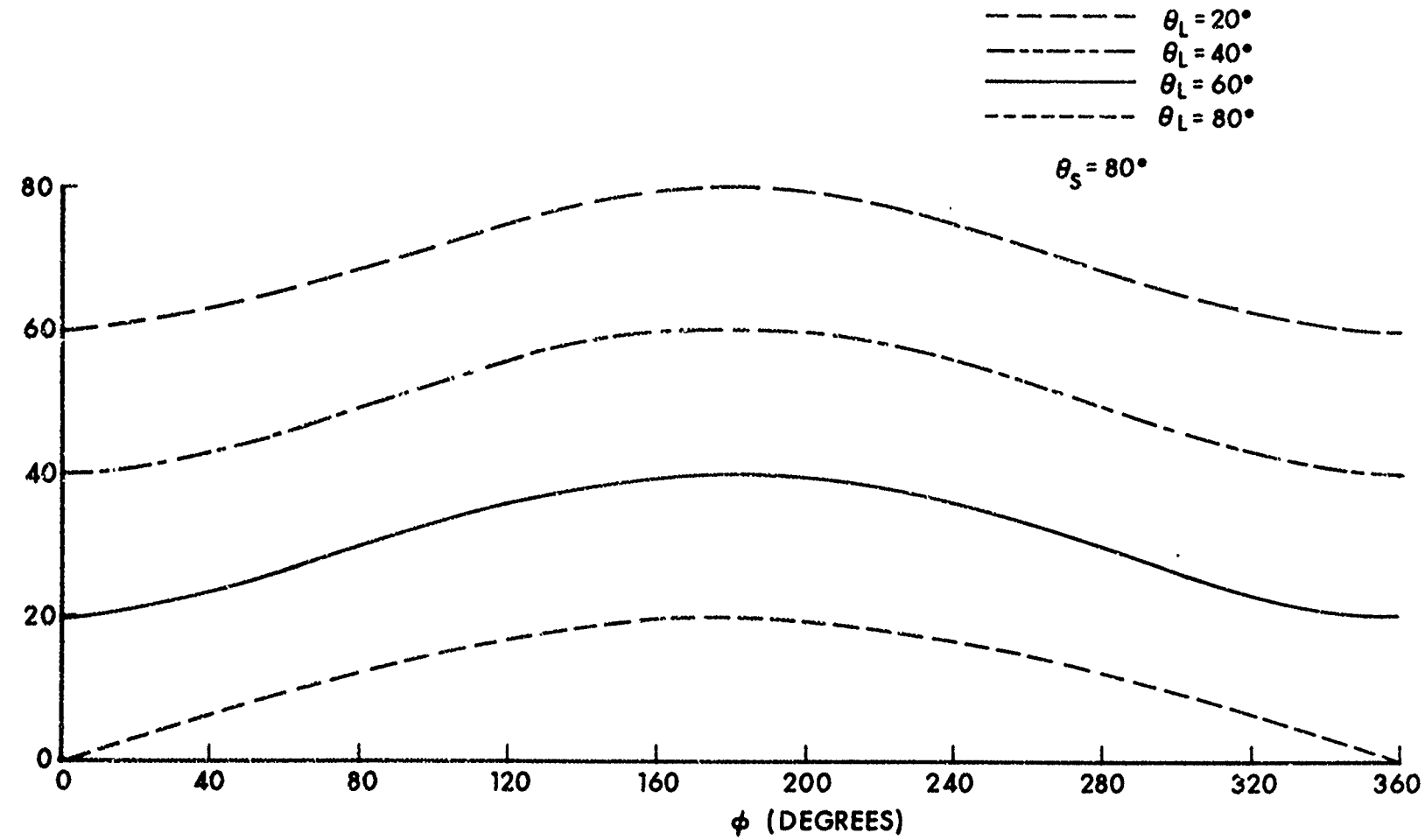

Figure 6. δ as a Function of θ_L and ϕ for θ_S = 80 Degrees.

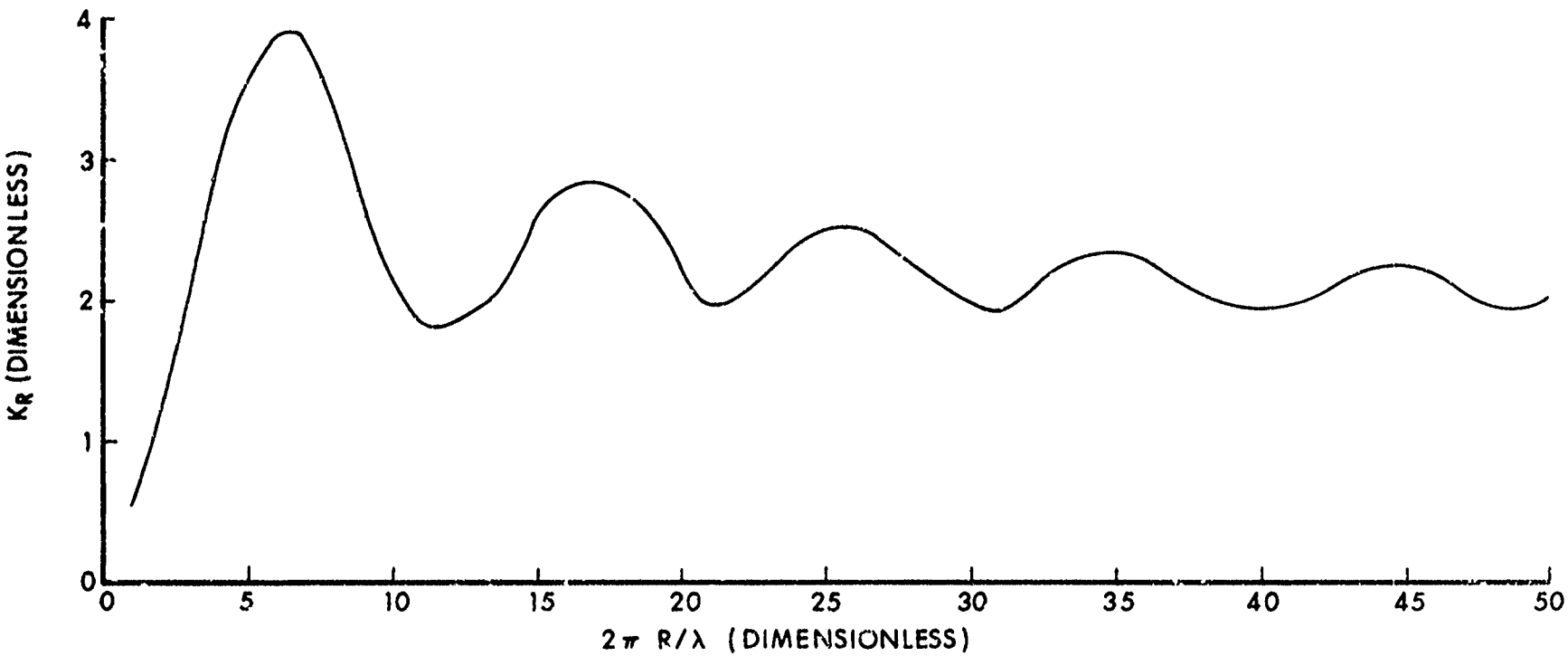

Figure 7. The Scattering Area Ratio as a Function of $2\pi R/\lambda$.

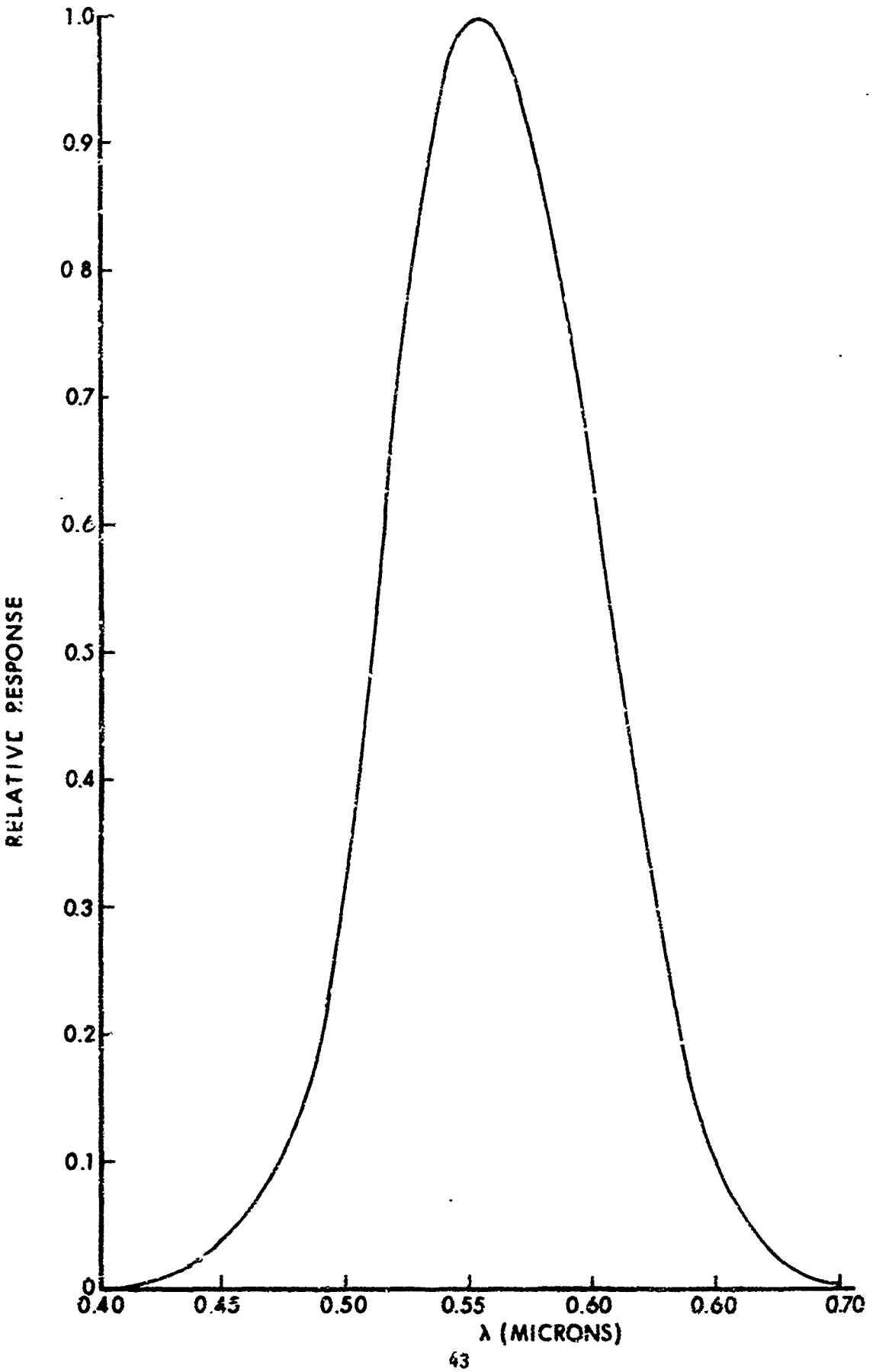

Figure 8. Relative Wavelength Response of the Human Eye.

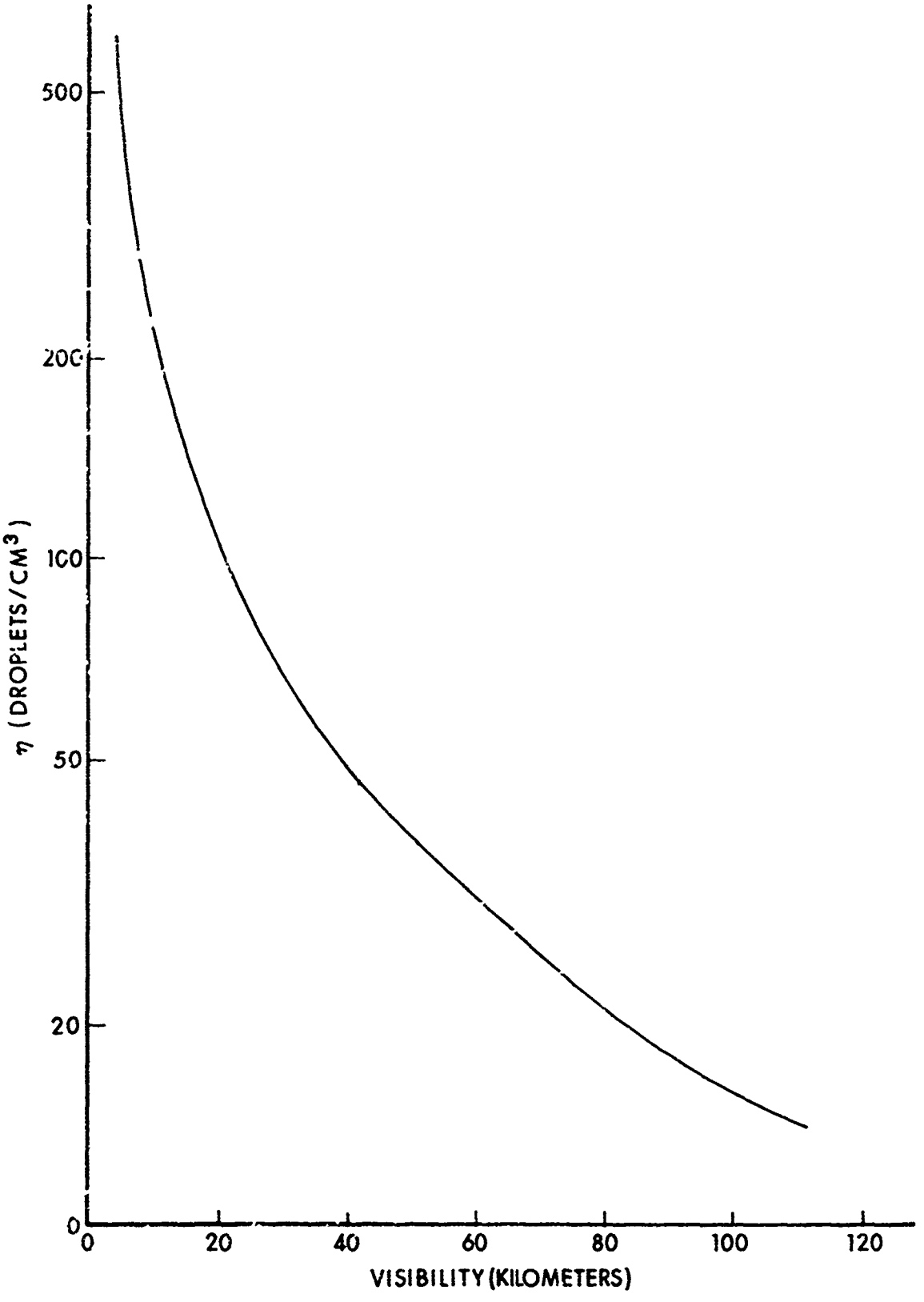

Figure 9. Droplet Concentration as a Function of the Visibility.

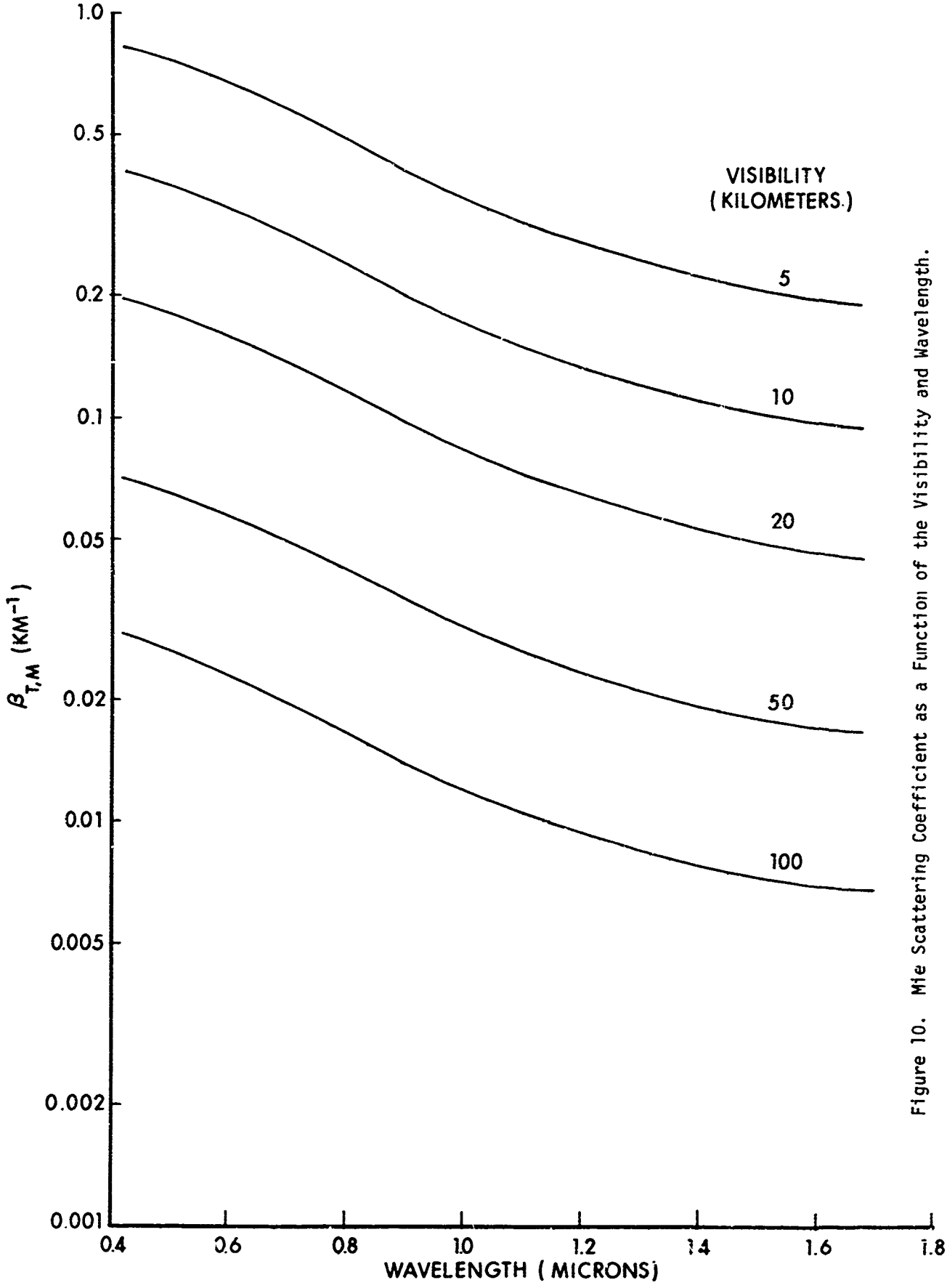

Figure 10. Mie Scattering Coefficient as a Function of the Visibility and Wavelength.

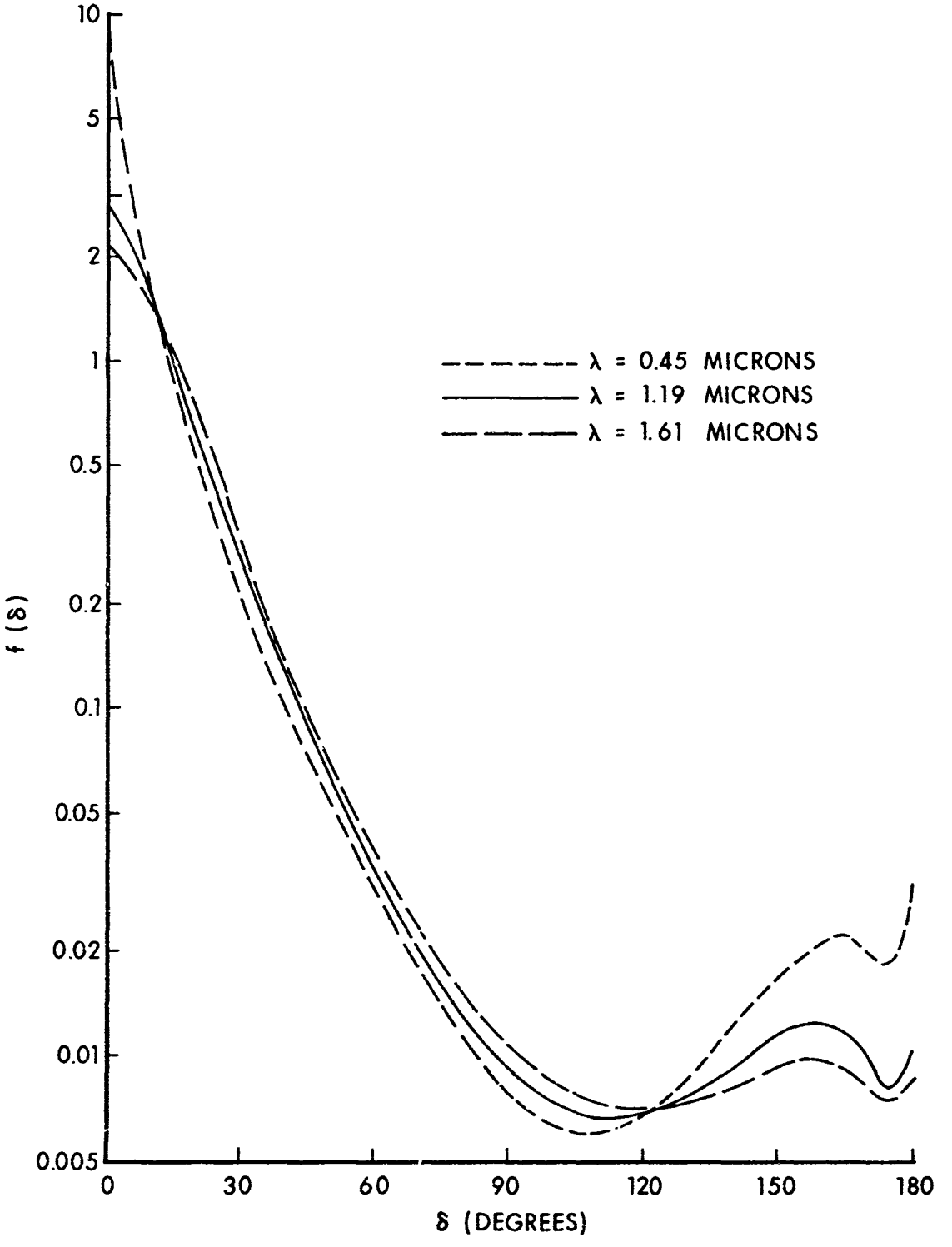

Figure 11. Normalized Directional Mie Scattering Coefficient.

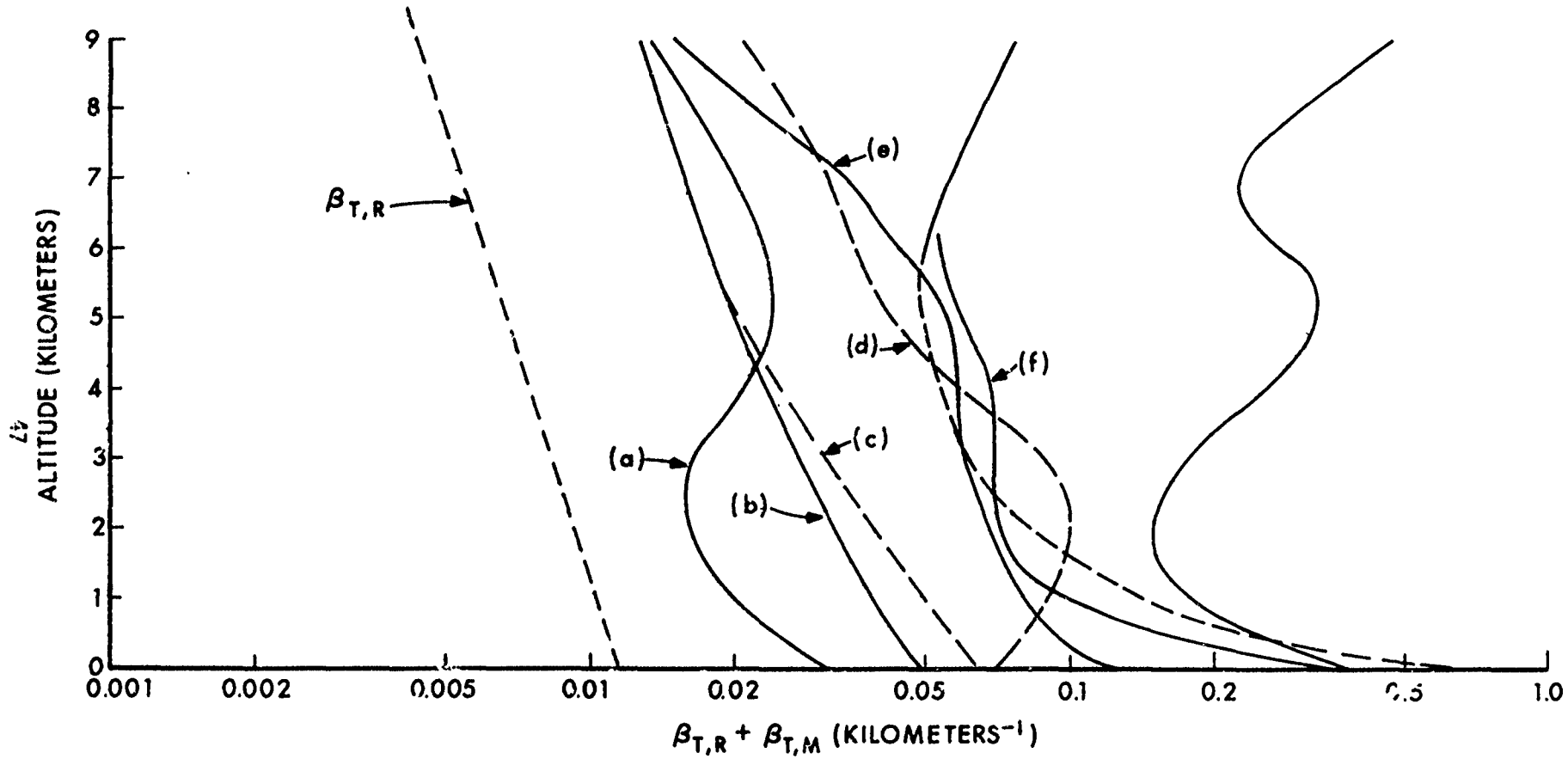

Figure 12. Altitude Variation of the Visual Spectrum Volume Scattering Coefficient after Waldram[14].

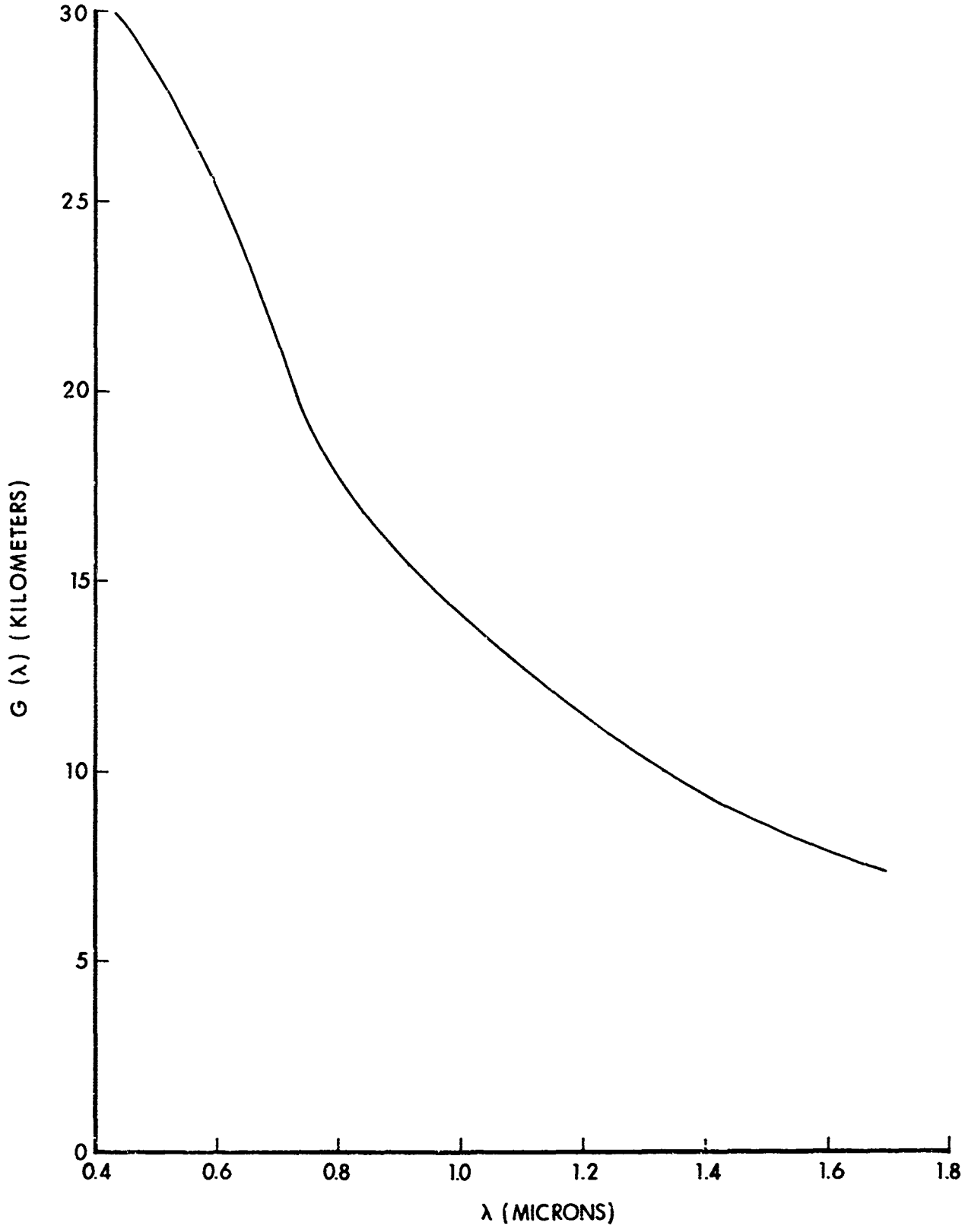

Figure 13. G(λ) as a Function of Wavelength.

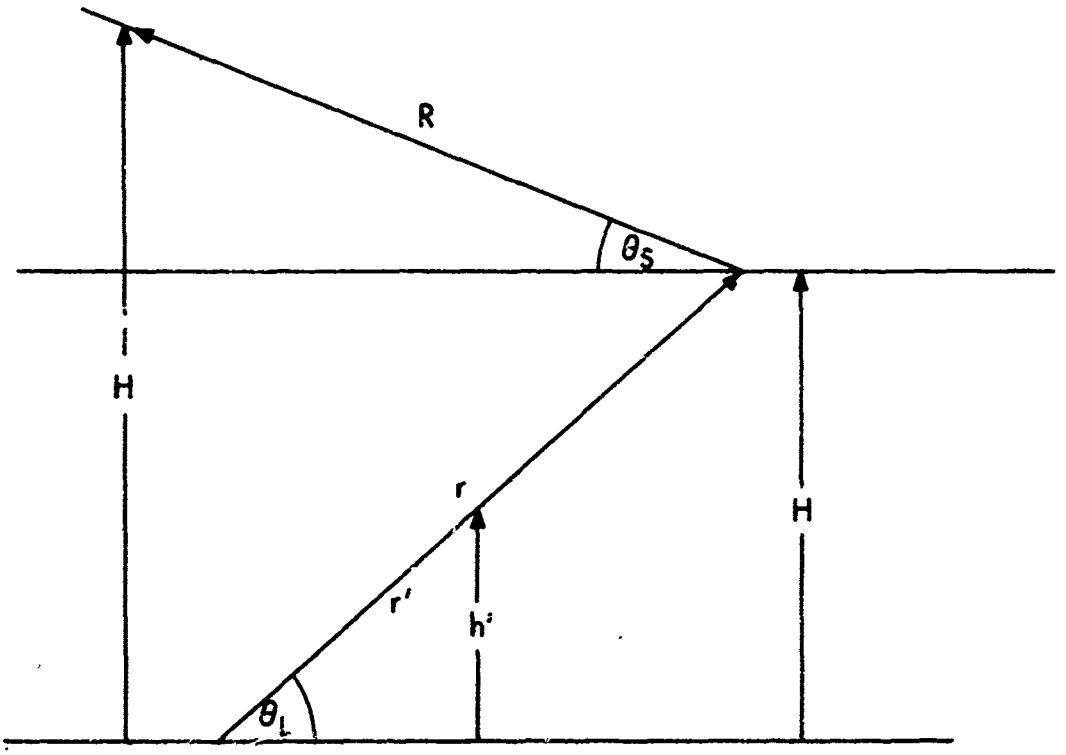

$$h' = r' \text{ SIN } \theta_L$$
$$h = r \text{ SIN } \theta_L$$
$$H = r \text{ SIN } \theta_L + R \text{ SIN } \theta_S$$

Figure 14. Mie Transmission Geometry for $V \geq G(\lambda)$.

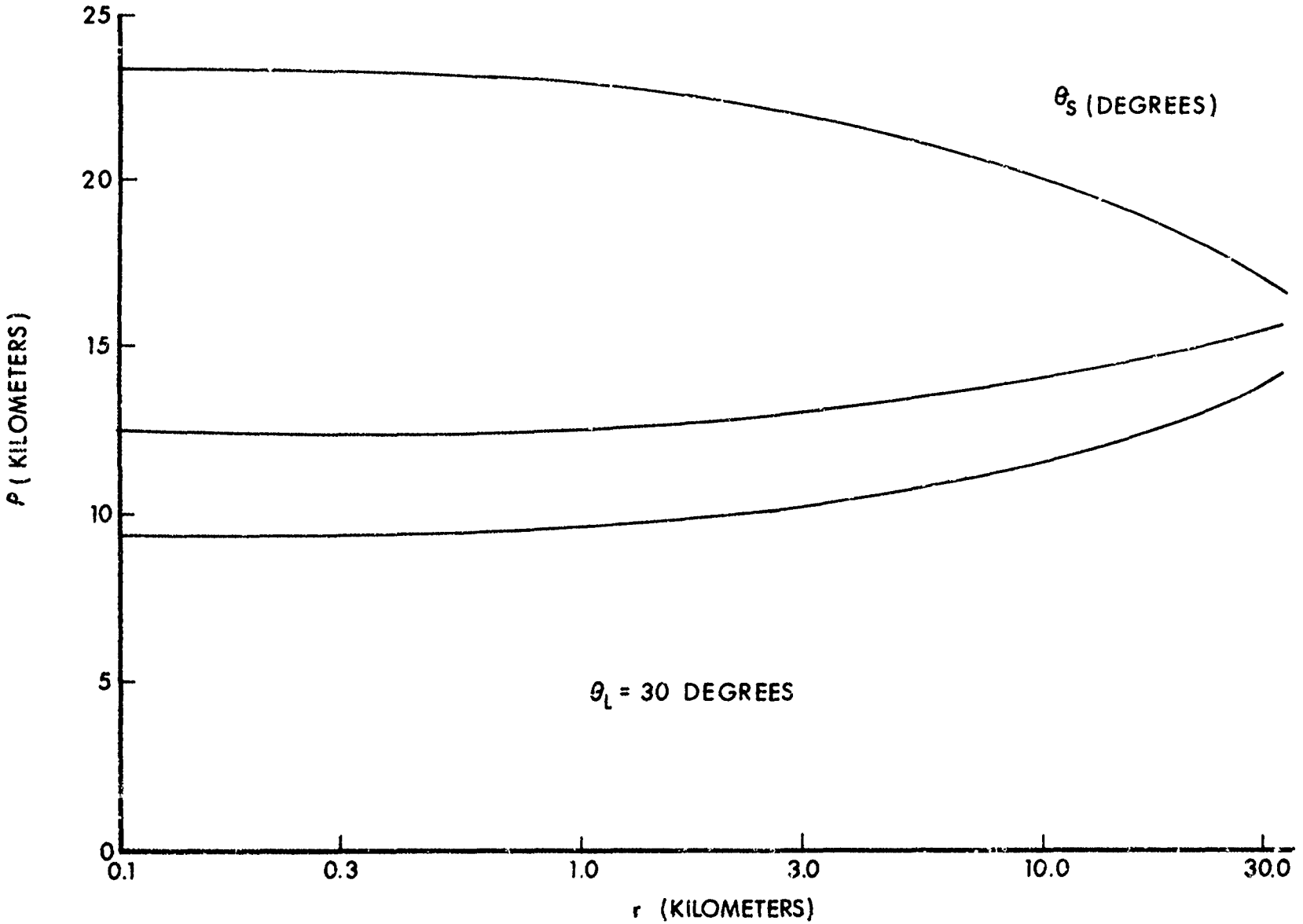

Figure 15. Carbon Dioxide Optical Slant Range as a Function of θ_s, θ_L, and r.

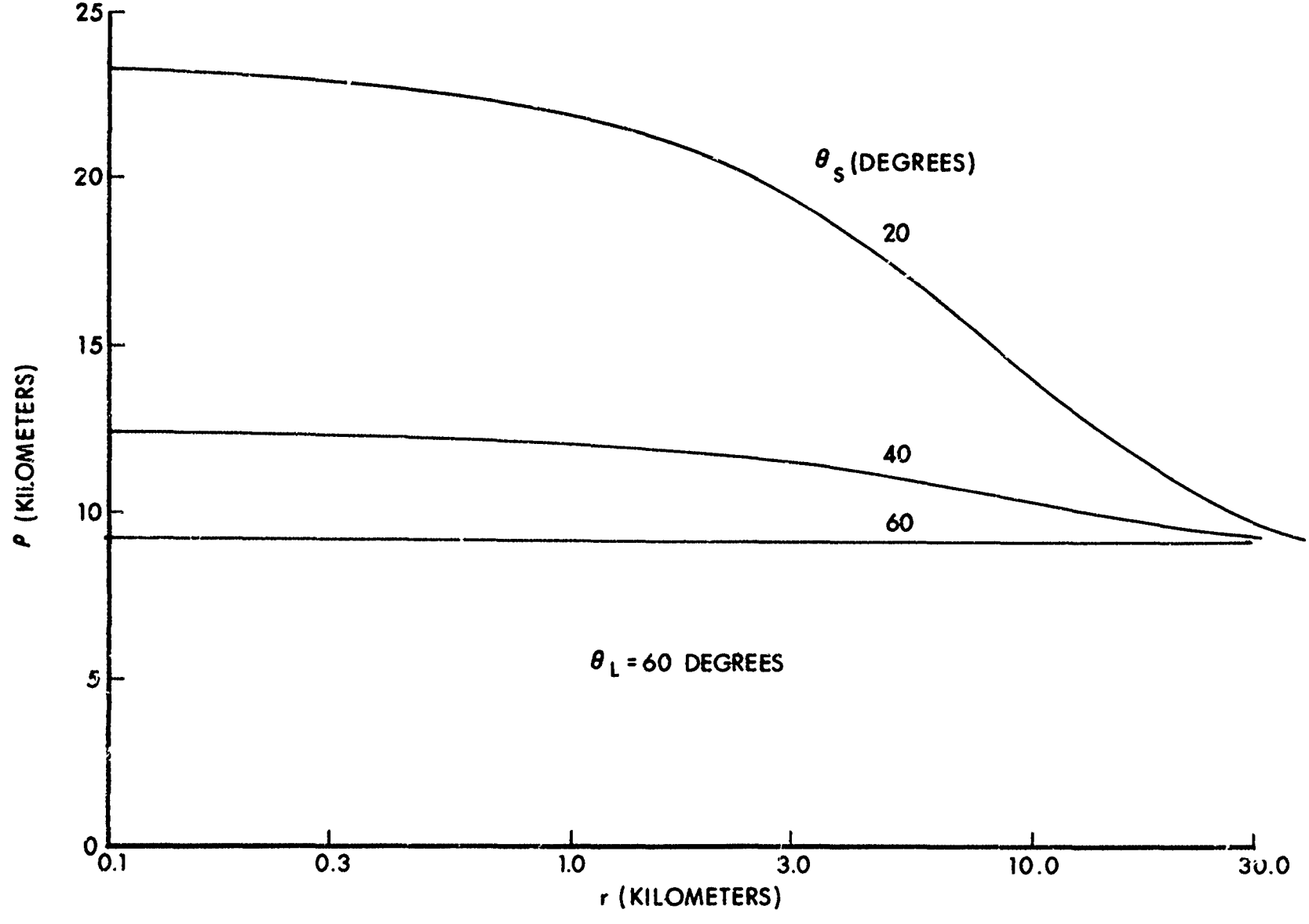

Figure 16. Carbon Dioxide Optical Slant Range as a Function of θ_s, θ_L, and r.

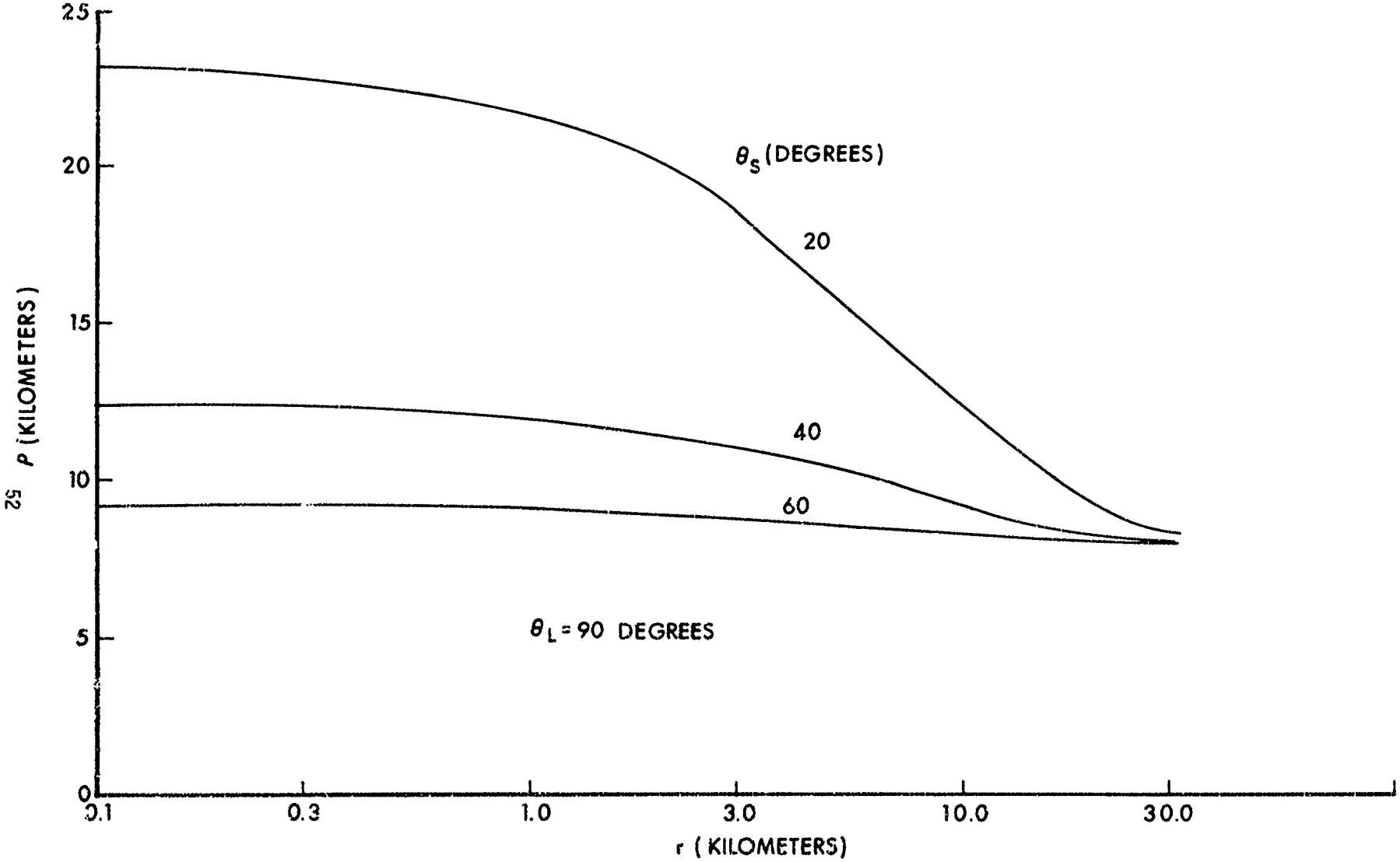

Figure 17. Carbon Dioxide Optical Slant Range as a Function of θ_S, θ_L, and r.

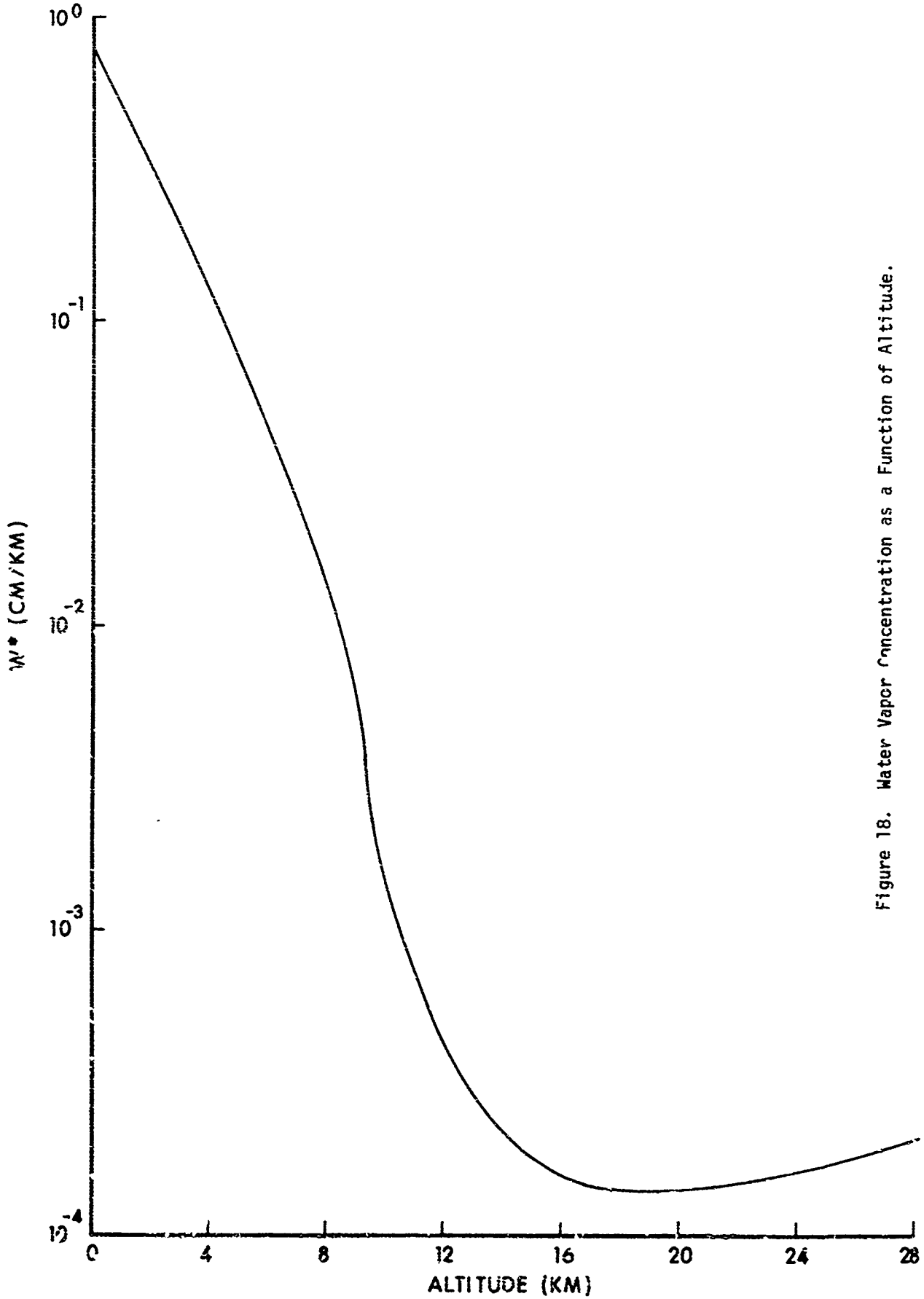

Figure 18. Water Vapor Concentration as a Function of Altitude.

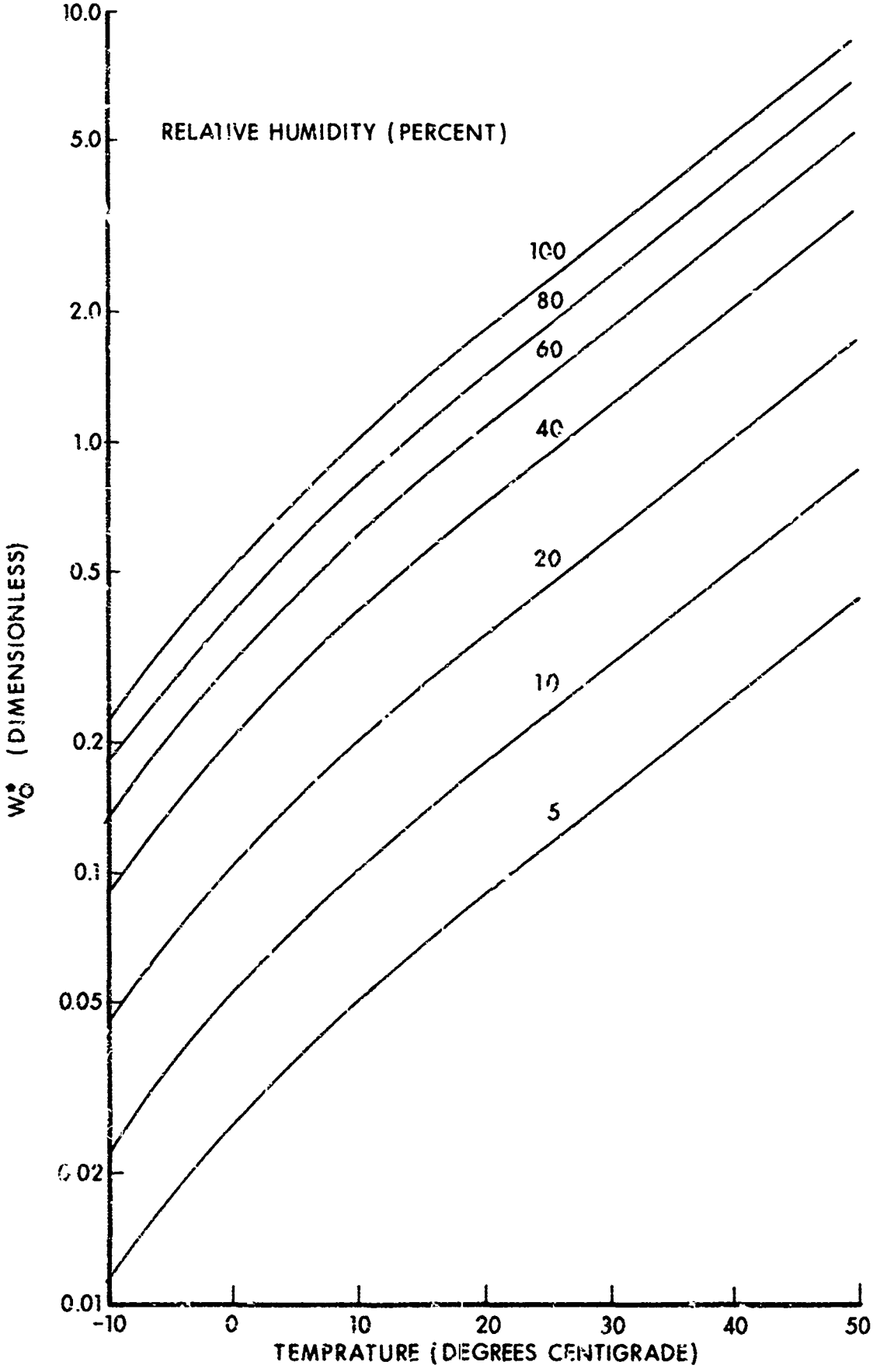

Figure 19. Water Vapor Concentration as a Function of Meteorological Conditions.

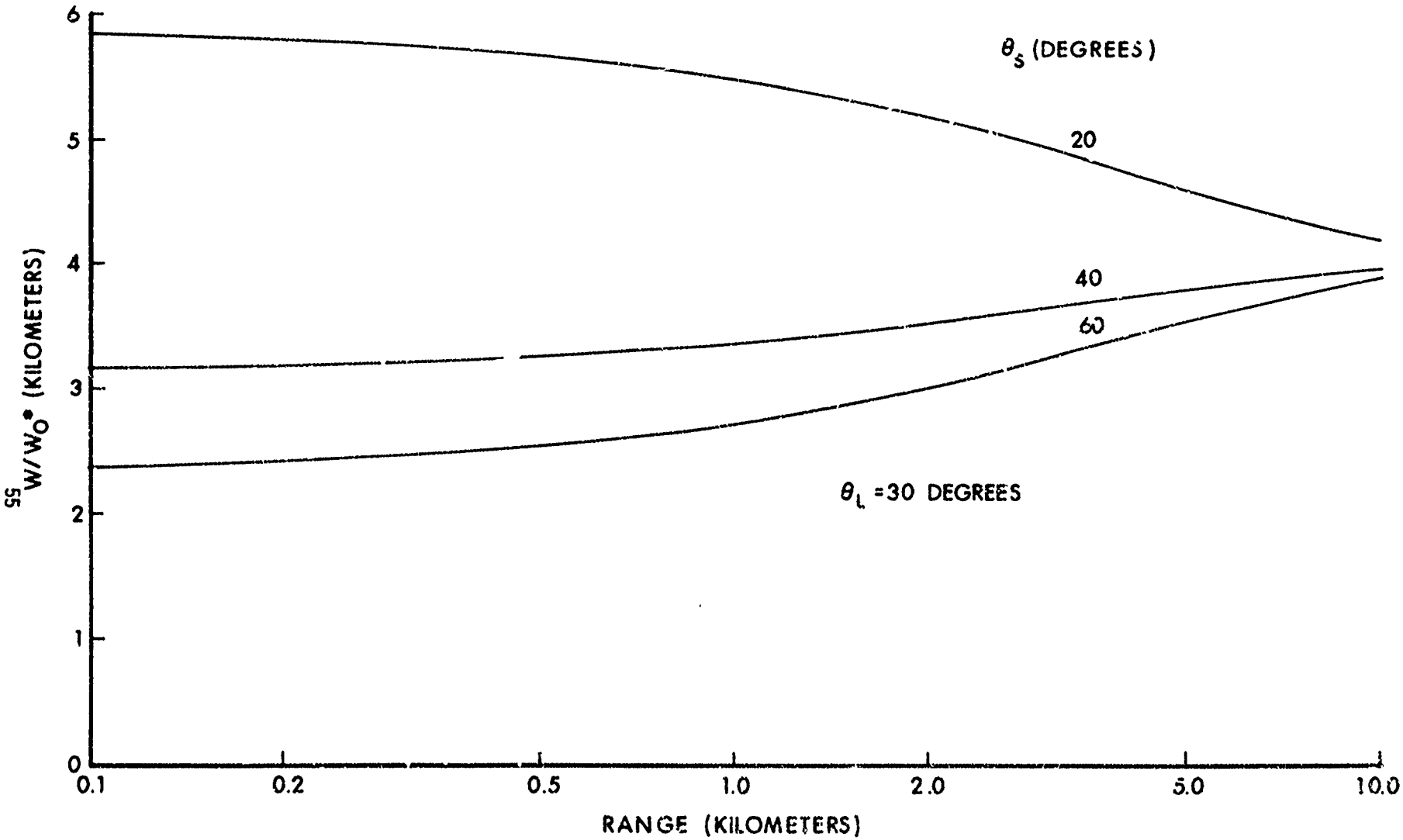

Figure 20. Water Vapor Optical Slant Range as a function of θ_s, θ_l, and r.

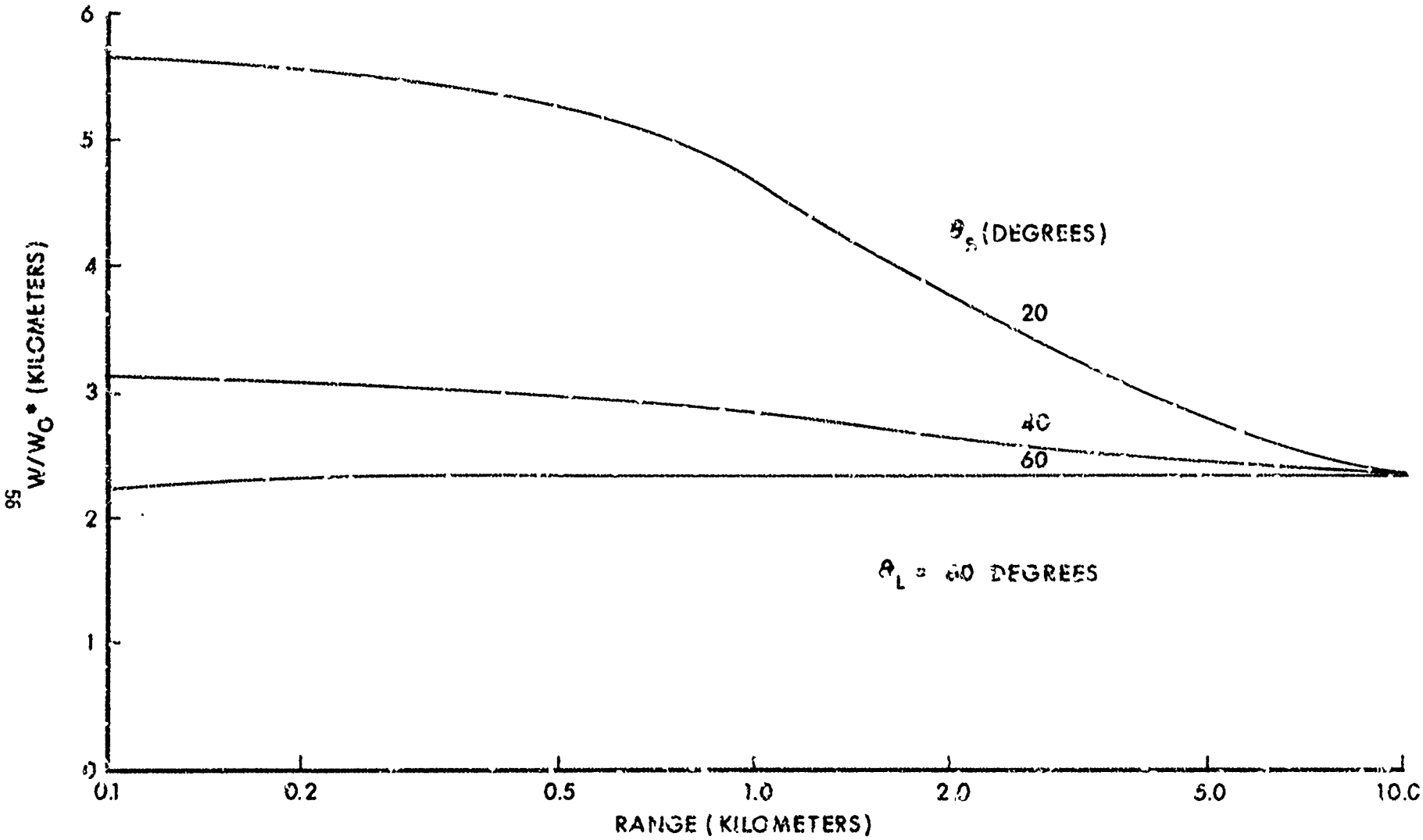

Figure 21. Water Vapor Optical Slant Range as a Function of θ_s, θ_L, and r.

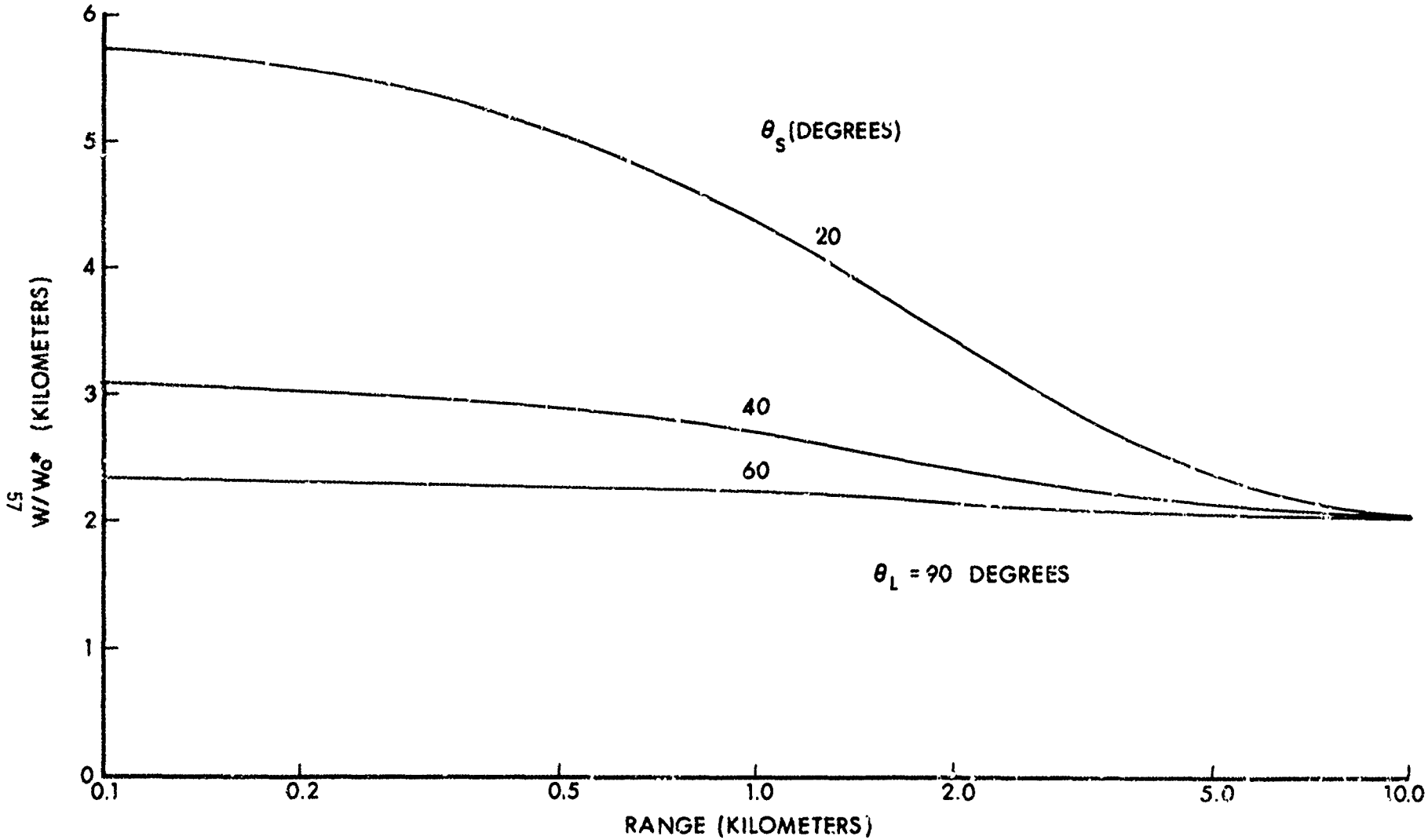

Figure 22. Water Vapor Optical Slant Range as a Function of θ_s, θ_L, and r.

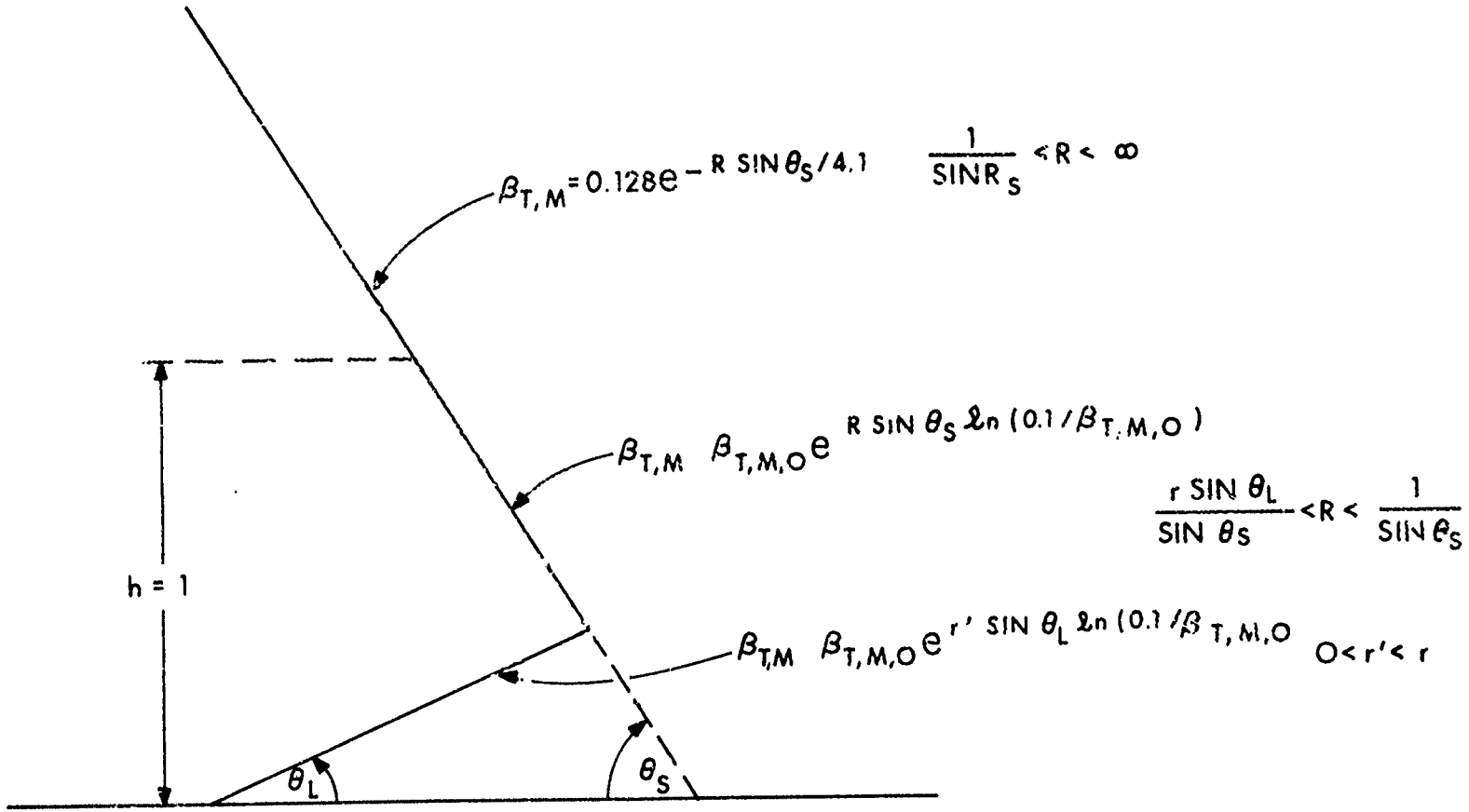

Figure 23. Mie Transmission Geometry for $V < G(\lambda)$ and $r < 1/\sin\theta_L$.

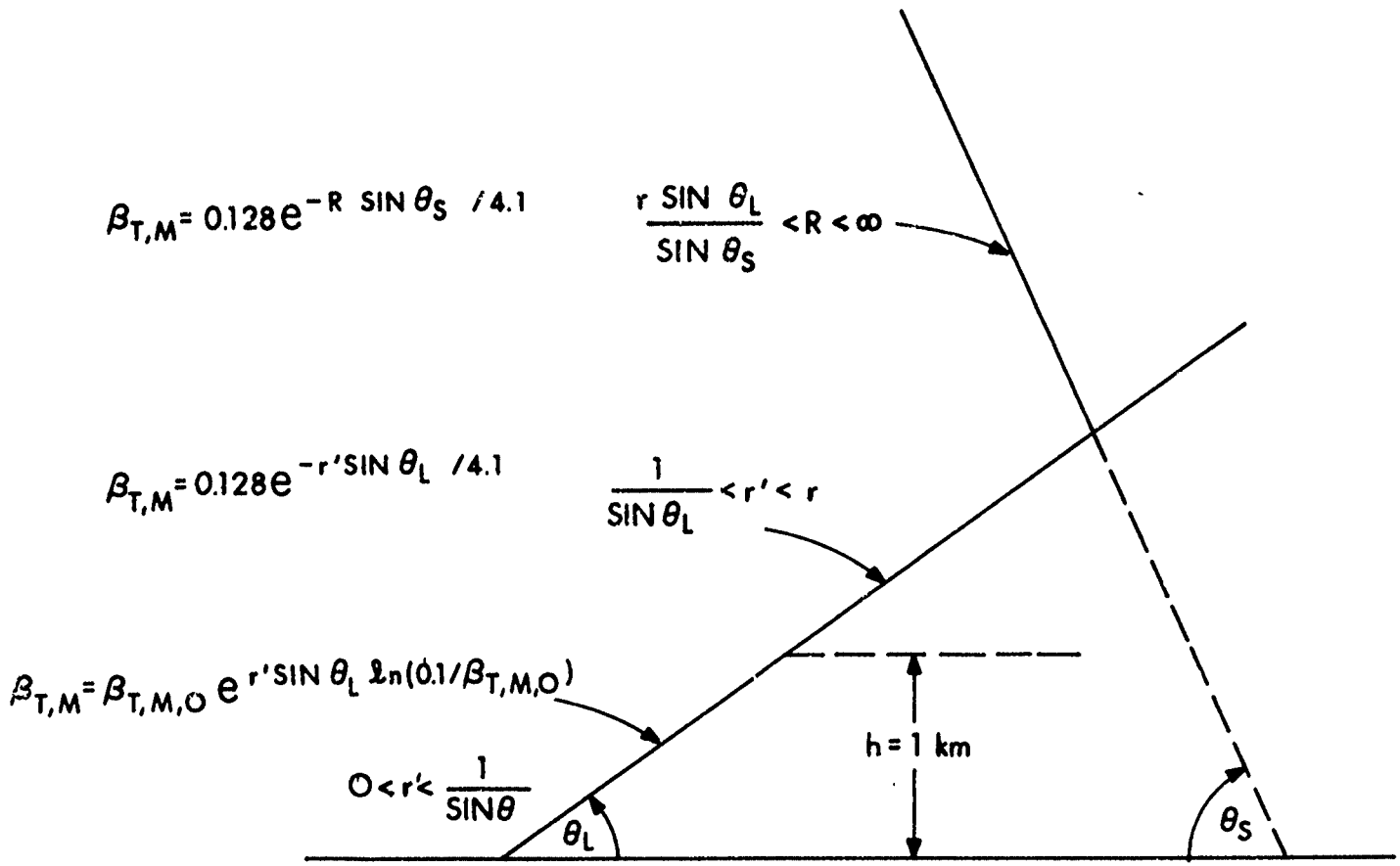

Figure 24. Mie Transmission Geometry for $V < G(\lambda)$ and $r > 1/\sin \theta_L$.

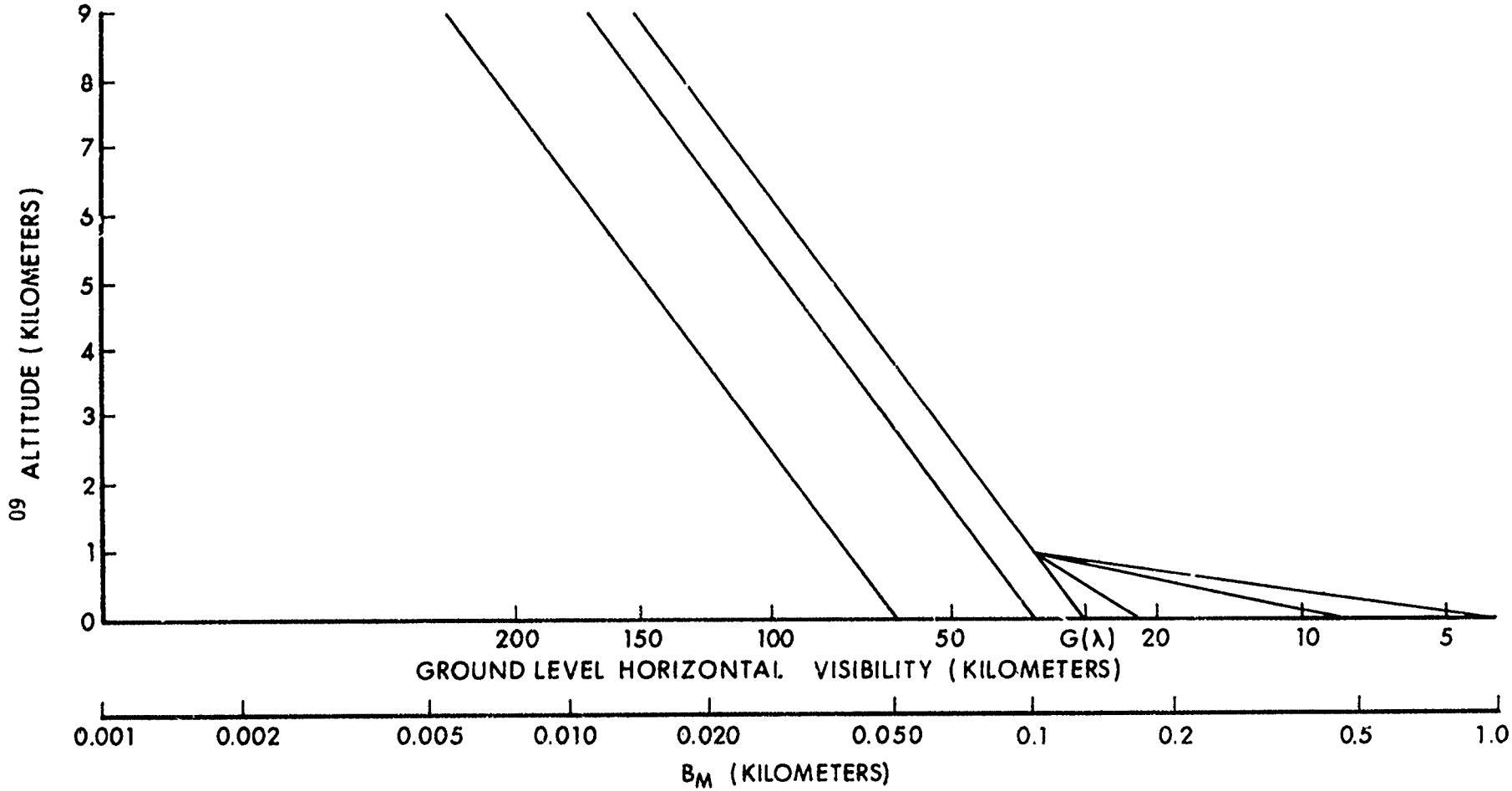

Figure 25. Altitude Variation of the Visual Spectrum Mie Volume Scattering Coefficient as Predicted by the Model.

TABLE I

$\Delta\lambda$ (Microns)	$H_s(\lambda)$ (10^{-3} w/cm^2)	$\frac{(n-1)^2}{\lambda^4_{cm}}$	$K_R(\lambda)$	$\alpha(\lambda)$	$\gamma(\lambda)$	g_λ	$\beta_{T,R}$
0.40-0.45	8.40	2.69×10^{10}	3.81	0	0.161	0.0054	0.0343
0.45-0.50	8.97	1.70	3.63	0	0.136	0.0615	0.0217
0.50-0.55	9.02	1.13	3.44	0	0.111	0.3437	0.0144
0.55-0.60	8.72	7.80×10^{9}	3.23	0	0.097	0.4164	0.0099
0.60-0.65	8.17	5.55	3.00	0	0.085	0.1582	0.0071
0.65-0.70	7.53	4.06	2.75	0	0.080	0.0149	0.0052
0.70-0.75	6.85	3.05	2.50	0	0.082		
0.75-0.80	6.19	2.33	2.27	0	0.090		
0.80-0.85	5.56	1.81	2.06	0	0.133		
0.85-0.90	4.98	1.43	1.90	0	0.266		
0.90-0.95	4.43	1.14	1.81	0	0.216		
0.95-1.00	3.96	9.24×10^{8}	1.72	0	0.096		
1.00-1.05	3.53	7.59	1.63	0	0.104		
1.05-1.10	3.16	6.22	1.54	0	0.214		
1.10-1.15	2.82	5.21	1.46	0	0.253		
1.15-1.20	2.53	4.36	1.38	0	0.195		
1.20-1.25	2.27	3.76	1.30	0	0.214		
1.25-1.30	2.04	3.15	1.23	0	0.505		
1.30-1.35	1.85	2.70	1.16	0.00214	0.753		
1.35-1.40	1.65	2.33	1.10	0.00846	0 829		
1.40-1.45	1.50	2.02	1.04	0.00779	0.957		
1.45-1.50	1.33	1.76	0.99	0.00282	1.106		
1.50-1.55	1.24	1.54	0.94	0.00282	1.120		
1.55-1.60	1.11	1.35	0.90	0.00779	1.044		
1.60-1.65	1.03	1.19	0.87	0.00846	1.003		
1.65-1.70	0.92	1.05	0.84	0.00214	0.904		